FEEDBACK LINEARIZED INDUCTION MOTOR CONTROL USING FOSMC AND SLIDING MODE-MRAS ESTIMATOR

MASTER OF SCIENCE IN CONTROL AND INSTRUMENTATION ENGINEERING

BY

YESHIWAS FETENE MENGESHA

HAWASSA UNIVERSITY, HAWASSA, ETHIOPIA

JULY, 2020

FEEDBACK LINEARIZED INDUCTION MOTOR CONTROL USING FOSMC AND SLIDING MODE-MRAS ESTIMATOR

BY

YESHIWAS FETENE MENGESHA

A THESIS SUBMITTED TO DEPARTEMENT OF ELECTRICAL AND COMPUTER ENGINEERING, HAWASSA INSTITUTE OF TECHNOLOGY, SCHOOL OF GRADUATE STUDIES.

HAWASSA UNIVERSITY
HAWASSA, ETHIOPIA

IN PARTIAL FULFILLMENT OF THE REQUIREMENTS FOR THE DEGREE OF MASTER OF SCIENCE IN CONTROL AND INSTRUMENTATION ENGINEERING

JULY, 2020

HAWASSA UNIVERSITY

INSTITUTE OF TECHNOLOGY

DEPARTMENT OF ELECTRICAL AND COMPUTER ENGINEERING

SCHOOL OF GRADUATE STUDIES

ADVISORS' APPROVAL SHEET

This is to certify that the thesis entitled "Feedback Linearized Induction Motor Control Using FOSMC and Sliding Mode-MRAS Estimator" submitted in partial fulfillment of the requirements for the degree of Master's with specialization in control and Instrumentation Engineering, The Graduate Program of the Department of Electrical and Computer Engineering, and has been carried out by YESHIWAS FETENE Id.no PGConR/009/10, under my supervision. Therefore, I recommend that the student has fulfilled the requirements and hence hereby can submit the thesis to the department.

Mr. Dereje Shibeshi	.....	.....
Advisor	Signature	Date

SCHOOL OF GRADUATE STUDIES

HAWASSA UNIVERSITY

EXAMINERS' APPROVAL SHEET

We the under signed Board of examiners of the final open defense by Yeshiwas Fetene have read and evaluated his thesis entitled "Feedback Linearized Induction Motor Control Using FOSMC and Sliding Mode-MRAS Estimator" and examined the candidate. This is therefore, to certify that the thesis has been accepted in partial fulfilment of the requirements for the degree.

Name	Signature	Date
Mr. Muluken Regassa Chair Person	_____	_____
Mr. Dereje Shibeshi Advisor	_____	_____
Dr. Eskinder Anteneh External Eximiner	_____	_____
Mr. Yeshitila Hialu Internal Examiner	_____	_____
_____ SGS	_____	_____

Final approval and acceptance of the thesis is contingent upon the submission of the final copy of the thesis to the school of graduate studies (SGS) through the department Graduate Committee (DGC) of Electrical and Computer Engineering.

Stamp of SGS .....

Declaration

I hereby declare that this MSc thesis is my original work and has not been presented for a degree in any other university and all the sources of materials used for this thesis have been fully acknowledged.

Yeshiwas Fetene — Student Name

 — Signature

This MSc thesis has been submitted for examination with my approval as thesis advisor.

Mr. Dereje Shibeshi — Advisor Name

_____ — Signature

Hawassa, Ethiopia

Date of Submission: July 13, 2020

Acknowledgment

First of all, I would like to thank GOD, the Most Gracious and the most Merciful, for blessing me with knowledge and giving me strength, courage and patience during the course of this study. Next, I would like express my deep gratitude to my supervisor, Mr. Dereje Shibeshi from Ethiopian Airlines, for his bright guidance and encouragement. I thank him so much that he was always there to support and advise me during the development of this thesis.

Last but not least, I would like to thank my parents pursuing and praying for my well being throughout their time.

Abstract

The Model of induction motor indicates that it is nonlinear, MIMO and strongly coupled system. To control this nonlinear motor as a nonlinear system, application of IOFL and sliding mode controllers are promising. Application of sliding mode controllers results the problem of chattering which is undesirable for electrical drive system. Here, this problem is tackled by using *sigmoid* function instead of *signum*. On the other hand, all states of squirrel cage induction motor are not easily accessible and use of mechanical speed sensor increases cost of the drive system. The proposed system eliminates the need of mechanical speed senor by employing combined Model reference adaptive system (MRAS) and sliding mode estimation technique which is known for robustness to model uncertainties and load disturbances. From simulation results carried out it is also observed that by using proportional integral derivative, sliding mode controller and fractional order sliding mode controller an overshoot of 9.5211%, 0.4753% and 0.3674% are found respectively for 120 rad/sec speed reference. FOSMC shows best robustness for load torque disturbance having a minimum speed drop of 1.1757% while PID and conventional integer order SMC have higher speed drop of 5.5982% and 1.388% respectively at the instant 10 Nm is applied. Application of sliding mode- model reference adaptive speed estimator gives good estimate of rotor flux with mean absolute percentage error of 0.2584% and speed with mean absolute percentage error of 0.1767%.

Key words: *Induction motor, Sensorless, IOFL, SM-MRAS, SVPWM, FOSMC*

Contents

List of Tables

List of Figures

List of Abberivations

AC	Alternating current
DC	Direct Current
FOSMC	Fractional order sliding mode control
IM	Induction motor
IOFL	Input output feedback linearization
KVL	Kirchofs voltage law
MIMO	Multiple input multiple output
MRAS	Model reference adaptive system
PI	Propotrional integral
PID	Proportional integral and derivative
SMC	Sliding mode control
SMO	Sliding mode observer
SVPWM	Space vector pulse width modulation
VSI	Voltage source inverter

List of Symbols

$(\alpha,\ \beta)$	Axes corresponding to the stator
$(d,\ q)$	Axes corresponding to the rotating field
$V_{sa},\ V_{sb},\ V_{sc}$	Three phase stator Voltages
$V_{ra},\ V_{rb},\ V_{rc}$	Three phase rotor Voltages
$V_{sd},\ V_{sq}$	Stator voltages in the frame $d-q$
$V_{s\alpha},\ V_{s\beta}$	Stator voltages in the frame $\alpha-\beta$
$i_{sa},\ i_{sb},\ i_{sc}$	Three phase stator currents
$i_{ra},\ i_{rb},\ i_{rc}$	Three phase rotor Currents
$i_{sd},\ i_{sq}$	Stator Currents in the frame $d-q$
$i_{s\alpha},\ i_{s\beta}$	Stator currents in the frame $\alpha-\beta$
$\lambda_{sa},\ \lambda_{sb},\ \lambda_{sc}$	Three phase stator fluxes
$\lambda_{ra},\ \lambda_{rb},\ \lambda_{rc}$	Three phase rotor fluxes
$\lambda_{sd},\ \lambda_{sq}$	Stator flux in $(d,\ q)$ coordinate system
$\lambda_{s\alpha},\ \lambda_{s\beta}$	Stator flux in $(\alpha,\ \beta)$ coordinate system
$R_s,\ R_r$	Stator and rotor resistances

L_s, L_r	Stator and rotor resistances
L_m	Mutual inductance between stator and rotor
f_r	Coefficient of friction
J_{eq}	Equivalent Moment of inertia
ω_m	Electrical angular speed
ω_{mech}	Mechanical angular speed
$f_{sa},\ f_{sb},\ f_{sc}$	Quantities in a, b, c frames
T_{em}	Electromagnetic Torque
T_l	Load Torque
p	Number of pole pairs

Chapter 1

Introduction

1.1 Background

Induction motors are the most prevalent motor in the industry today, which constitute more than 85 % of all industrial machines [1]. DC motors were extensively used in variable speed applications since their flux and torque are independently controlled by the field and armature current. However, they since have mechanical commutator and the brushes they are limited in applications which needs high speed, voltage operating conditions. Induction motors are much more difficult to control but have the following definite advantages [2]:

- have no commutator and brushes
- have no rotor windings in squirrel cage motors
- have a simple and rugged mechanical structure.
- can resist heavy overloading and.
- can produce higher torques with a lower weight, smaller size, and lower rotating mass than DC motors

The aim of many researches nowadays is to achieve the same, or even superior, performance on speed tracking and power efficiency which are obtained by more

sophisticated and expensive, but less reliable, electric motors such as direct current or permanent magnet ones by induction motors [3].

In earlier times, induction motors have been operated directly from the power grid with a fixed frequency/speed. Later, with the emerging development of modern semiconductor technology and power electronic converters, it becomes easier to operate these machines with adjustable frequency/speed by using power electronic converter like the voltage source inverter (VSI) [4]. AC machine control in general can be categorized into scalar and vector control. Scalar control is the simplest scheme applied to control the speed of IMs based on constant ratio of voltage and frequency using the steady state equivalent circuit model of the machine. However, this method does not dedicate for high performance applications due to its slow response and the existence of coupling between torque and flux. To solve these problems, vector control can be used. Vector control was invented at the beginning of 1970s. It can be used with both induction and synchronous machines to transform the control of an AC machine in to more likely to that of a separately excited DC motor. The vector control method has also the advantage of fast torque response compared to other variable-speed control technique. Vector control method has been commonly applied to drive the induction motor accurately, and for the advantages of lower cost and smaller size [5, 6, 7].

Higher order models of AC machines, nonlinearities in model equations, uncertainties in parameters and load disturbances are the main obstacles hindering the development. The mathematical analysis of such items is rigorous. As shown in Figure 1.1, modern induction motor drive controller has sensor, controller, inverter, and induction motor. From the blocks it can be seen that the overall technique of controlling those machines involves understanding of three main electrical engineering areas: control system, power electronics, and electrical machines [8].

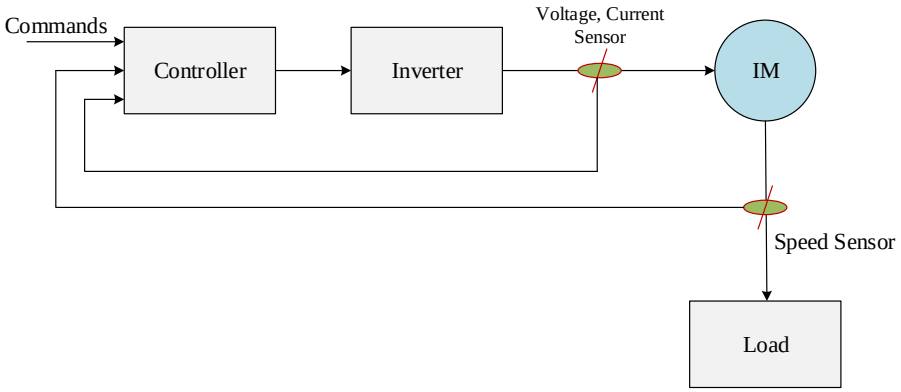

Figure 1.1: Induction motor control

Developing a control algorithm for induction motors is however very complex for many reasons. A challenging problem occurs due to the following three reason: It is a highly nonlinear dynamic system, some electrical variables such as rotor flux and currents are not easily measurable, and some physical parameters (rotor and stator resistance) vary considerably with a significant impact on the system dynamics. It is a MIMO control problem since there are two independent inputs and two outputs to be controlled.

Controlling of induction motors have been mostly done by using field orientation, assuming the rotor flux is entirely aligned on a specific axis and fixed at a constant value. Even though this assumption can result in better decoupling of flux and torque, it can't guarantee for high performance control as it is difficult to get rotor flux entirely aligned on an axis [7] and this technique is not robust for parameter variation [2]. For this reason it is necessary to search for another controller suited for this system. In recent years, the nonlinear systems control theory has raised a very great interest. Among nonlinear controllers available in literature, input output feedback linearization is applied to get a fully decoupled controller for the torque and the flux dynamics and is found to have better tracking capability of electrical drive controllers [9]. Feedback linearization transforms the original MIMO nonlinear system in to a linear decoupled equivalent system as long as the matrix of decoupling

is non-singular. This latter acts an important role in the motor's performance. In addition, it also reduce the control algorithm complexity.

However, the major shortcoming associated with input output feedback linearization is it needs all the states as feedback by measurement which results increase of measurement sensors cost [10]. This shortcoming can be handled by using effective state estimator. If rotor speed is not measured in order to reduce costs or due to sensor failures and only stator currents and voltages are available from measurements, the control problem is called sensorless speed control [3]. Among the estimation techniques, Model Reference Adaptive System (MRAS) , rotor flux based one in particular, is one of the most attractive adaptive control technique used for motor control and state estimation application [11] because of its simplicity. Estimation using MRAS is based on the comparison of the outputs of the two models. Then, the calculated error is used to drive an adaptation mechanism that generates the desired estimated quantity (Rotor speed in general cases).The performance of MRAS speed estimation is highly dependent on the type of adaptation mechanism controller used.

Sliding mode control (SMC) is a well-known nonlinear variable structure control technique that forces the system state trajectory to reach a predefined stable surface (called the sliding surface) within a finite time and subsequently drives it to the origin asymptotically along the surface. The dynamical behavior of the system when the state trajectory is confined to the sliding surface is called the sliding mode. SMC is a robust controller in the sense that during ideal sliding mode, the system dynamics is independent of plant parameters and hence invariant to parametric uncertainty [12, 13]. Chattering effect is a remarkable disadvantage of sliding mode controller because of the presence of *signum* function. This problem can be solved by approximating it with some other contionous functions like saturation or sigmoid functions. In recent past, several literature have shown that fractional order controllers can perform better than their integer order counter parts because of their adjustable orders of derivative and integration which adds an additional degrees of freedom to the controllers. FOSMC uses the concept of fractional calculus for developing a controller.

Fractional calculus deals with the generalized differentiation and integration for any arbitrary non-integer order [14].

This thesis work focuses on sensorless control of squirrel cage induction motor which is found to be highly nonlinear MIMO system by applying input output feedback linearization techniques to decouple rotor flux and developed electromagnetic torque well. For the speed controlling loop fractional order sliding mode controller (FOSMC) is applied to track the desired speed in a short period of time and with minimized steady state error using fractional order sliding surfaces as is proposed in [12, 14, 15, 16]. The general structure of the proposed closed loop system is depicted as in Figure 1.2:

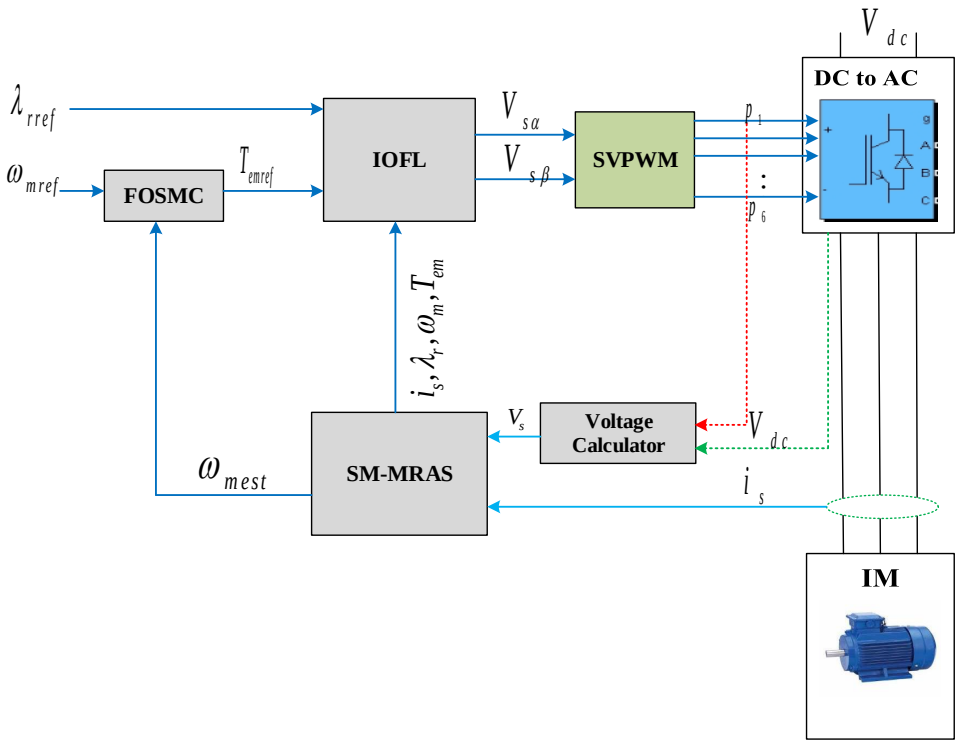

Figure 1.2: Block diagram of the proposed control structure

1.2 Statement of the Problem

Vector control with fixed gain PI and PID controllers has been mostly applied to achieve the controlling task of AC motors. This control mechanism is based on dq frame model and orienting rotor flux entirely on an axis keeping its magnitude constant which as a result linearizes the machine model partially and makes controlling easier. But in practice it is difficult to get the rotor flux totally aligned on a fixed axis and literatures show that vector controlling is prone to coupling at low speed and parameter variations for this control scheme. Even though PID controllers are the easiest controller, their performance is not reliable under uncertainties and load disturbances.

Nonlinear controllers are now becoming the best choice of high performance drive controlling application because of their fast tracking performance and robustness to variations. For the speed controlling loop the commonly used PI characterized by sever overshoots and higher sensitiveness to variations can be replaced by sliding mode controller for fast tracking and enhance robustness to load variations. Recent works proved that fractional order sliding mode controller (FOSMC) not only deal with robustness to parameter variations but also track the desired trajectory faster than conventional integer order SMC surfaces. The major drawback of using sliding mode controllers is the chattering (undesirable oscillation) present due to utilization of signum function. This problem of chattering phenomenon can be alleviated by using smooth continuous approximation in place of the discontinuous function. On the other hand, input output feedback linearization needs all states as feedback requiring measurement sensors for each state. It is also impossible to measure even some states of squirrel cage induction motor like rotor flux.

Even though it is possible to use high resolution speed encoders for speed measurement, it increases the drive cost and makes the system prone to mechanical failure. The above mentioned problems motivates replacement of those sensors with appropriate estimation algorithm that can extract speed from stator current and voltage

information. To solve this problem, speed has been estimated by various techniques. The most commonly used estimator for high range rotor speed estimation is rotor based flux MRAS. But, this estimator is still having problems estimating in low speed regions. Literatures show that, better estimate of rotor speed can be obtained using this estimator by improving the reference model and its adaptation mechanism.

1.3 Objectives

1.3.1 General Objectives

- To develop mathematical model of squirrel cage IM and sensorless fractional order speed controller based on feedback linearization of induction motor using space vector pulse width switching scheme for inverter switching and model reference adaptive rotor flux observer based on sliding mode adaptation.

1.3.2 Specific Objectives

- To model the nonlinear dynamical behavior of squirrel cage induction motor
- To formulate sensorless speed estimation algorithm using sliding mode model reference adaptive system.
- To apply fractional order sliding mode speed controller and feedback linearization for better decoupling.
- To simulate the overall system using MATLAB/SIMULINK software.

1.4 Scope of the Work

The scope of this thesis is developing mathematical model of the motor and sensorless speed control of squirrel cage induction motor using sliding mode control scheme and

sliding mode model reference adaptive system for speed and flux estimation. Controlling task is going to be done via input output feedback linearization for flux and torque decoupling. Fractional order sliding mode controller is going to be applied by selecting fractional order sliding surface. Derived mathematical designs are simulated in MATLAB/SIMULINK environment and clarification with plain discussions will be presented.

1.5 Methodology

The proposed sensorless fractional order sliding mode speed control of feedback linearized induction motor is shown in figure 1.2. To arrive at the final goal of this work, the following steps are followed:

From the beginning, the task is to start with modeling of squirrel cage induction motor. At this stage, nonlinear MIMO dynamic equations representing the physical system into a mathematical form is derived. After having the model the next attempt is to control speed of induction motor using appropriate technique for the proposed system. Literatures show that input output feedback linearization (IOFL) not only handle problems of commonly used vector and direct torque controllers applied for this motor but also results good tracking capability with best decoupling ability. At this point IOFL for perfect decoupling of electromagnetic torque and rotor flux is studied. This enables to control flux and torque separately. The remaining task is to control the speed of Squirrel cage IM motor. In this thesis speed controlling is going to be done by using a fractional order sliding mode controller (FOSMC) proved to have best robustness and minimized chattering than conventional integer order sliding mode controller (SMC). IOFL needs all the states to be feedback and this increases the measurement sensors. For IOFL to remain still the best choice, the required measurement sensors should be minimized by replacing it with an appropriate state estimator.

The next task focuses on study of robust speed estimator (sliding mode MRAS)

that can eliminate the need of mechanical speed encoder and flux measurement sensors. Here, improvement and stability of estimation will be gained by combining the two observers. The inputs to estimator are stator currents and voltages. To reduce the measurement devices the proposed system uses an algorithm for calculation of stator voltages using measured DC input voltage to the inverter and three basic SVPWM switching pulses. Finally, clear analysis depending on MATLAB simulation result will be given and checking of responses to different speed and references with and without load disturbances is going to be done. Summarized representation of methodology to be followed is presented in the flow chart below.

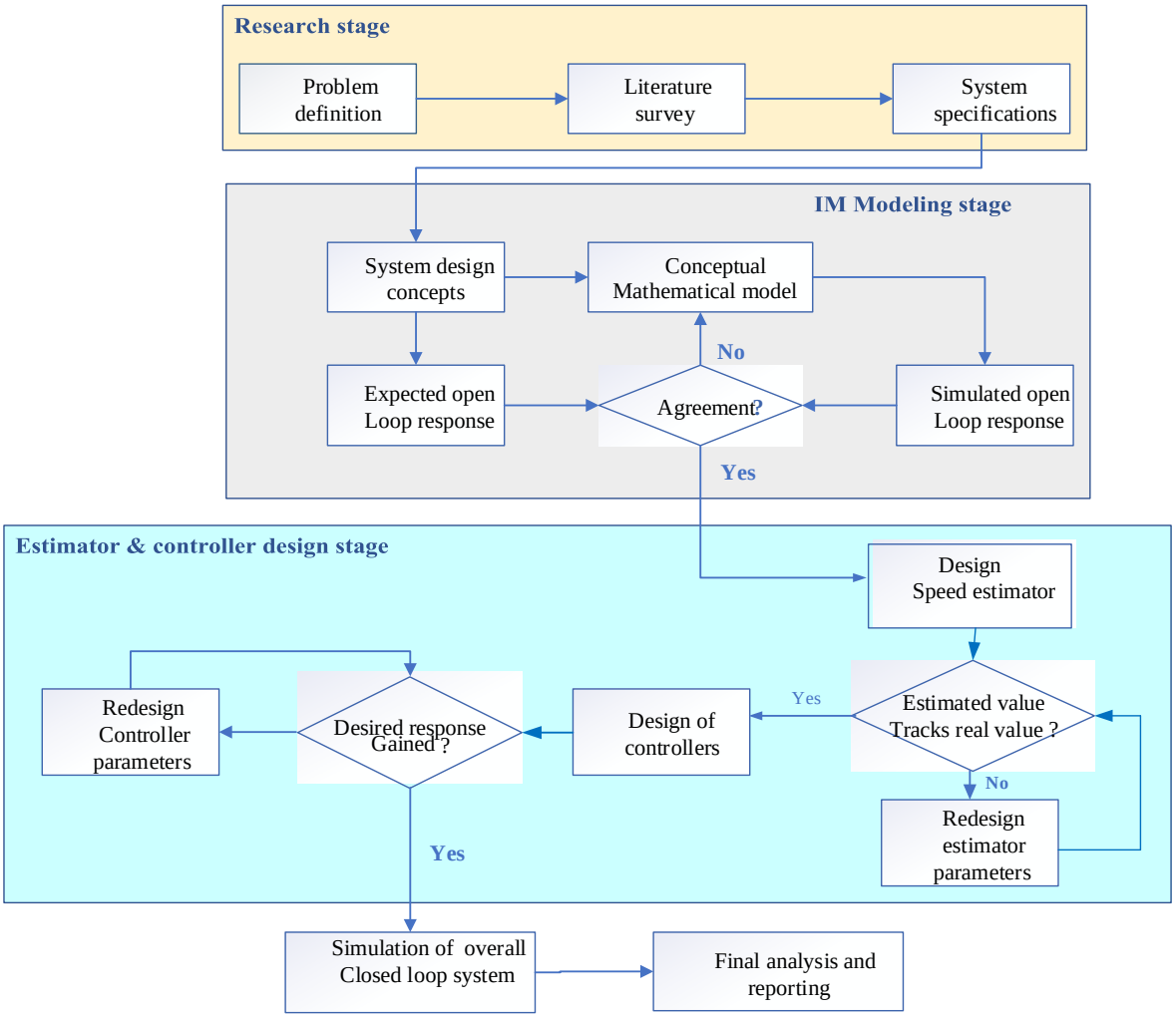

Figure 1.3: Methodology of the proposed system

1.6 Contribution of Thesis

This thesis work is done considering nonlinear behavior of squirrel cage induction motor with no need of complex transformation to partially linearize it using field orientation and eliminating the need of speed, flux and stator voltage measurement sensors.

Here are the main contributions of this thesis:

- Input output feedback linearization controller is obtained for fully decoupled controlling of rotor flux and electromagnetic torque dynamic of induction motor, based on FOSMC speed controller.
- Speed encoder which is the cause of frequent mechanical failures and maximizing the drive cost and flux sensors are replaced by using SM-MRAS estimator and stator voltage measurement is not required as it is calculated from SVPWM pulse gates and DC input voltage of the inverter.
- Robustness to load torque disturbance is guaranteed and minimal chattering controller is developed by using continuous approximation for sliding mode controller.

1.7 Outline of the Thesis

The thesis is organized into six chapters including this introduction. The rest of the thesis will be presented as follows.

Chapter 2:Literature Review

This chapter reviews some important concepts and previously accomplished works related to this thesis.

Chapter 3:Model of Induction Motor and SVPWM

This chapter studied the model of induction motor. It briefly describes about induction motors and focuses on the modeling of this motor based on coordinate transformation and its SVPWM to drive the controlling inverter. Two types of models of

this motor namely model on the rotating frame and model on the stationary frame are presented. This chapter also presents the open loop responses and discussions of the modeled system at the end.

Chapter 4: Modeling of controller and estimator

In this chapter the application of SM-MRAS estimator and controllers of the proposed system is addressed. Here detail derivations are presented based on input output feedback linearization of rotor flux based sliding mode-model reference adaptive system. Speed controller and load torque estimator are also discussed.

Chapter 5: Simulation Results and Discussion

This chapter discussed on the overall simulation of the drive system on MATLAB/Simulink including simulation results. Included in this chapter, simulation results based on different speed commands and load torque disturbance are discussed.

Chapter 6: Conclusion and Future Work

Draws the conclusion from the works done in this thesis and indicates further possible improvements which can enhance the overall performance of this drive system.

Chapter 2

Literature Review

2.1 Introduction

Speed control of IMs, the squirrel cage in particular, has become a hot topic of interest for the last few years. To achieve high-performance application control for IMs, different books, articles and journals have been reported for modeling, analysis and control of those machines in various ways.

2.2 Review of Sliding Mode Controller

2.2.1 Integer order sliding mode controller

Sliding mode controller is a specific type of variable structure control technique applied to achieve two objectives. Firstly, it drives the nonlinear plant's state trajectory on to a specified and user chosen surface in the state space which is called the sliding surface. Secondly, it maintains the plants state trajectory on this surface for all subsequent times [13].

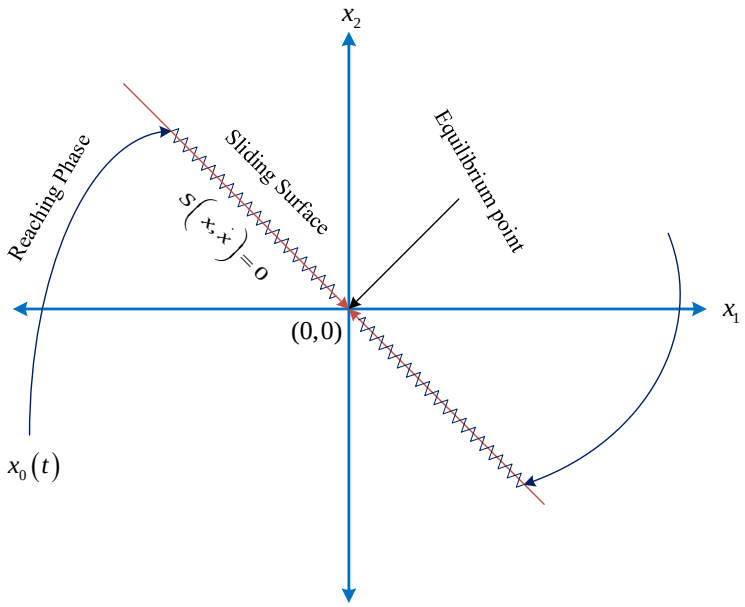

Figure 2.1: Sliding mode control operating modes in the phase plane

The trajectory in the phase plane consists the two important conditions of sliding mode control.

Reaching mode: This is the mode during which the variable to be adjusted moves at from any initial point in the phase plane, and tends towards the surface of switching $S\left(x,\dot{x}\right)=0$

Sliding mode: This is the mode during which the state variable has reached the sliding surface and tends towards the origin of the phase plane. The dynamics of this mode is characterized by the choice of sliding surface $S\left(x,\dot{x}\right)$

2.2.2 Fractional Order Sliding Mode Controller

Before discussing FOSMC, a brief review of fractional calculus seems necessary. Fractional calculus has been known since the development of integer order calculus. The idea has begun by Leibniz's question "Can the meaning of derivatives with integer order $\frac{d^n y(x)}{dx^n}$ be generalized to derivatives with non-integer orders?" by his letter to L'Hospital in 1695 [17]. Mathematical definitions of fractional order integrals and

derivatives have been addressed by different scholars. Fractional calculus is generalized by the operator ${}_aD_t^\alpha$ where a and t denote the limits of the operation α denotes the fractional order of integrator or differentiator. A generilized representation of integration and derivation can be denoted as:

$$ {}_aD_t^\alpha = \begin{cases} \frac{d^\alpha}{dt^\alpha} & for \quad \alpha > 0 \\ 1 & for \quad \alpha = 0 \\ \int_a^t (d\tau)^\alpha & for \quad \alpha < 0 \end{cases} \tag{2.1} $$

2.2.3 Fractional operators, definitions and properties

There exists several definitions of fractional operator [18].

i **Grunwald-Letnikov definition:** One of the most frequently encountered definition is called Grunwald-Letnikov definition and is expressed as follows:

$$ {}_aD_t^\alpha = \lim_{h \to 0} h^\alpha \sum_{j=0}^{n} (-1)^j \begin{pmatrix} \alpha \\ j \end{pmatrix} f(t - jh) \tag{2.2} $$

Where the binomial coefficients are

$$ \begin{pmatrix} \alpha \\ 0 \end{pmatrix} = 1, \quad \begin{pmatrix} \alpha \\ j \end{pmatrix} = \frac{\alpha (\alpha - 1) .... (\alpha - j + 1)}{j!} \quad for \quad j \geq 1 $$

and $nh = t - a$

ii **Riemann-Liouville definition:** Another most widely used definitions of fractional order calculus is Riemann-Liouville definition with an integro-differential expression. The definition for fractional order integral is:

$$ {}_aD_t^{-\alpha} = \frac{1}{\Gamma(\alpha)} \int_a^t (t - \xi)^{\alpha - 1} f(\xi) \, d(\xi) \tag{2.3} $$

While the definition of fractional derivative is:

$$ {}_aD_t^{\alpha} = \frac{d^{\gamma}}{dt}\left[{}_aD_t^{-(\gamma-\alpha)}\right] \tag{2.4} $$

Where

$$ \Gamma(x) = \int_0^{\infty} y^{x-1}e^{-y}dy $$

is the Gamma function and γ is an integer that satisfies $\gamma - 1 < \alpha \leq \gamma$.

iii **caputo definition:** Another definition of generalized fractional order derivative and integral operator is Caputo's definition. It is presented as follows.

$$ {}_aD_t^{\alpha} f(t) = \frac{1}{\Gamma(n-\alpha)} \int_a^t \frac{f^n(\tau)}{(t-\tau)^{(\alpha+1-n)}} dt \tag{2.5} $$

Where $\alpha \in R, \quad n \in N \quad and \quad n-1 < \alpha \leq n$

Among these definitions discussed above, Grunwald definition is the most popular one and the work in [19] has led to a user friendly MATLAB/SIMULINK toolbox called FOMCON. This thesis also uses this definition as Simulations of the fractional order sliding mode control part are going to be verified with use of this toolbox.

2.2.3.1 Properties of Fractional calculus operator

Fractional order operator has the following properties [20].

1. For $\alpha = n$, where n is an integer, the operation ${}_aD_t^{\alpha} f(t)$ gives the same result as classical differentiation.

2. For $\alpha = 0$ the operation ${}_aD_t^{\alpha} f(t)$ is an identity operator.

$$ {}_0D_t^0 f(t) = f(t) \tag{2.6} $$

3. Fractional differentiation and integration are linear operations.

$$ {}_aD_t^{\alpha}\left(af\left(t\right)+bg\left(t\right)\right)=a\,{}_aD_t^{\alpha}f\left(t\right)+b\,{}_aD_t^{\alpha}g\left(t\right) \tag{2.7} $$

4. Semi-group property

$$ {}_aD_t^{\alpha}\left({}_aD_t^{\beta}f\left(t\right)\right)={}_aD_t^{\alpha+\beta}f\left(t\right) \tag{2.8} $$

5. Fractional order derivative shows commutative property with integer order derivatives.

$$ \frac{d^n}{dt^n}\left({}_aD_t^{\alpha}f\left(t\right)\right)={}_aD_t^{\alpha}\left(\frac{d^n}{dt^n}f\left(t\right)\right)={}_aD_t^{n+\alpha}f\left(t\right) \tag{2.9} $$

2.2.4 Application of Fractional order Calculus in Sliding mode control

Even though the concept of fractional calculus is older, it has been considered as a sole mathematical problem. It was only in in the last two decades that its application in the field of engineering came into practice in control applications. Exploration of fractional order counterparts of the existing control algorithms became an area of interest for control engineering practitioners due to the additional flexibility and precision that it offers, owing to its adjustable order of derivative and integration. As SMC is known for its robustness and is opted to control many real world systems, researchers are nowadays introducing fractional order calculus to get better performance of this controller. The application of fractional order sliding surface is implemented in [12] for magnetic levitation system and in [15] for position control of permanent magnet synchronous motor. Results from these research works reveals that FOSMC outperforms SMC in terms of tracking accuracy, speed of response, and chattering. The aim of this thesis is thus to maintain the robustness property of SMC

controller and bring these improvements.

2.3 Related Works

In 2014 S. M. Gadoue, D. Giaouris, W. Finch [21] presented with Performance Evaluation of a Sensor less Induction Motor Drive at Very Low and Zero Speed Using MRAS Speed Observer. This work aims to evaluate the performance of rotor flux-based speed estimator at nearly zero speed during both loaded and unloaded conditions. This paper also informs that Rotor flux based MRAS sped estimator has comparatively better performance than other MRAS schemes especially in medium and high-speed regions. This paper clearly justifies that the operation of sensorless drives in general deteriorates in low speed region and becomes extremely unstable during loaded operation. The major causes of this problem are signal acquisition errors, Inverter non-linearity, Distortions in the flux angle, incorrect speed estimation, pure integration problems, and Parameter variations. At low speeds, a steady state error in the estimated speed is observed due to the stator resistance mismatches between motor model and estimator. In this work, the reference model is the commonly used voltage model and adaptive model is taken as current model and the mechanism used for adaptation is PI controller. To test the performance of this estimation rotor flux MRAS scheme this paper applies a step change command of 20 to 0 RPM at 20% load and from the responses observed this scheme fails to estimate lower speeds or does not provide stable operation rather it gives larger oscillations. The results from this paper indicates that even though MRAS has better performance in higher speed regions it needs improvements to equip it to have a quality of better performance in all operating speeds of the motor.

In 2014 M. Salima, T.Riad, B. Hocine [22] presented input output feedback linearization technique aiming to improve the field oriented control scheme. According to this paper DC machines played an important role in the early days of high performance electrical drive systems, since the magnetic flux and torque are easily

controlled by the stator and rotor current, respectively. To bring a similar controlling approach to induction motors vector control or field oriented control was introduced by Balaschke in 1970s. But, this control technique has a great weakness since it needs the exact knowledge of the machine model in (d, q) reference frame, a low robustness against the parametric variations of the machine, and in addition with this mode of control loss of decoupling occurs in low speed. To improve the weakness of field Oriented Control, authors of this work applied a new controller based on the theory of input output feedback linearization and presented clear comparative study between vector control and the proposed linearization control technique in terms of their ability to handle load disturbances, speed tracking capability, sensitivity to variations in the operating conditions. The concept of input output feedback linearization (IOFL) was applied in a way to make the outputs y_j follow a desired trajectory transforming the algebraically nonlinear system dynamic into a linear one cancelling its nonlinearities by using appropriate control laws using MIMO nonlinear model of squirrel cage induction motor of the form:

$$\begin{cases} \dot{x} = f(x) + \sum_{i=1}^{p} g_i(x).u_i \\ y_j = h_j(x) \qquad\qquad 1 < j \leq m \end{cases} \tag{2.10}$$

Where $x \in R^n$ is the state vector, $u \in R^p$ is control input vector, $y \in R^m$ output vector, f and g are smooth vector fields on R^n , and h is smooth vector field on R^m .

The basic modeling concept in IOFL is achieving decoupled dynamics and generate the original input based on nonlinear state feedback transformation by successive derivation of outputs until at least one of the inputs appear in the result. To validate the performance of the proposed controller and make comparison to the classical field oriented control, authors of this work provided a series of simulations in MATLAB/SIMULINK environment. In the paper, it is concluded that input output linearizing controller shows better performance than the field oriented controller in speed tracking at high speed ranges under load torque disturbance and parameter

variations.

In 2015 M. Zaky S. Khater, M. Yasin, H. Shokralla [23] presented on review of different speed estimation schemes for sensor less induction motor drive. The paper presents the currently available estimation techniques and presents their corresponding merits and demerits as well as their feasibility for rotor speed estimation. Currently available estimation techniques are compared according to some set of criteria which allow assigning the merits that can be used to choose the proper method depending on the specific application. According to this review paper, sensorless speed-controlled drives are the choice of next generation drive system usually by using terminal motor quantities stator voltages and currents and rarely injecting signals to stator terminals.

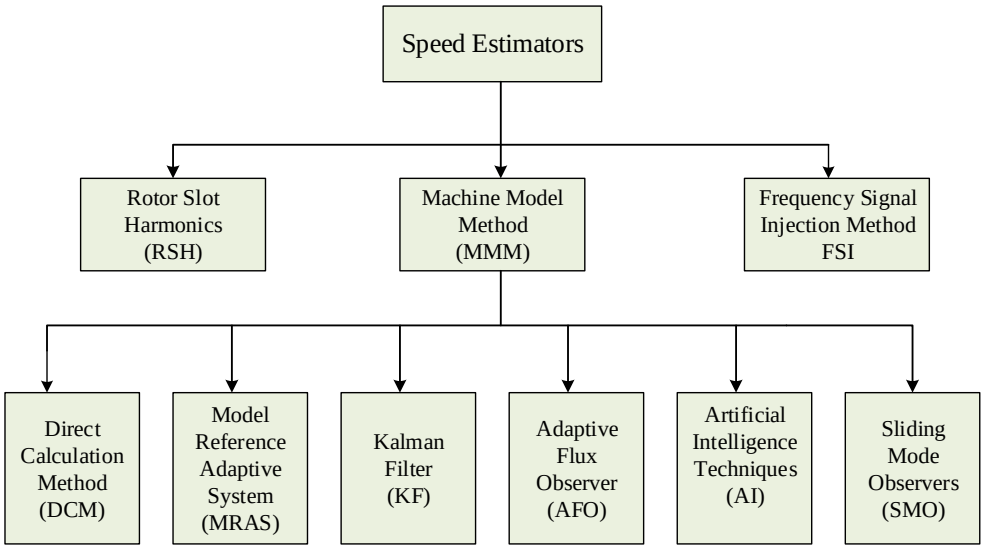

Figure 2.2: Speed estimation techniques of sensor less system

Speed estimators can be categorized in to two main categories, non-model and model based techniques. In the current time, model based techniques have attracted most of researchers because of their simplicity. This paper informs the importance of MRAS since it leads to relatively easy-to-implement systems with high speed of adaptation for a wide range of applications. Authors of this paper presented clear comparison between different speed estimation methods according to the set of cri-

Table 2.1: Comparison of different speed estimation methods

Method \ Criteria		SSE	DB	LSO	PS	NS	C	CT
RSH		2	3	1	1	4	5	3
FSI		2	2	1	1	4	5	3
MMM	DCM	2	3	4	4	4	2	2
	MRAS	2	3	4	3	4	2	3
	KF	2	2	2	2	1	5	5
	AFO	2	1	3	3	2	2	2
	AI	1	1	2	1	2	3	4
	SMO	1	1	2	1	2	2	2

teria which has been chosen to assign the merits for each presented speed estimation technique as summarized shortly in Table 2.1. In the table, criteria used to compare different speed estimators are steady state error (SSE), dynamic behavior (DB), low speed operation (LSO), parameter sensitivity (PS), and noise sensitivity (NS).

1, 2, 3, 4, 5 are weighted to mean Excellent, very good, good, satisfactory, and weak respectively or 1 means best behavior while 5 means poorest behavior. From the table, low speed estimation problems encountered in many speed estimation techniques can be solved by using the two non-model based methods, rotor slot harmonics or fast signal injection methods but, they are found to be complexity of implementation and prone to noise and have less popularity now a days. Kalman filter can be used for less noise sensitivity but it is also complex and takes longer computation time. In addition linearity plays an important role in its derivation and performance of KF hence it is not mostly recommended to use for nonlinear systems. This paper informs the importance of MRAS since it leads to relatively easy-to-implement systems with high speed of adaptation for a wide range of applications. From Table 2.1, it can be concluded that SMO offers good behavior with respect to all proposed set of criteria. Therefore easy-to-implement and wide range speed estimation capability of MRAS can be enhanced further by incorporating it with SMO which have the most promising responses in terms of steady state error, dynamic behavior and parameter sensitivity.

In 2017 N. Bouarroudj, D. Boukhetala, F. Boudjema [16] presented Sliding mode controller based on fractional order calculus for a class of nonlinear systems. This work addresses the concepts of both conventional integer order sliding mode controller (SMC) and fractional order sliding mode controller (FOSMC). According to this paper advantages such as robustness to parameter variations and external disturbances makes sliding mode control an effective tool in various applications. The first step in sliding mode controller modeling is selecting the desired sliding surface that models the desired closed loop performance in the state space model. The second step is driving an equivalent control law such that the system state trajectories are forced towards the sliding surface and slide along it to the desired attitude.

FOSMC basically augments the concept of sliding mode controller (SMC) by incorporating fractional order dynamics in to it. In the paper, simulation results were provided for the case of controlling an inverted pendulum system. The effectiveness and robustness of the proposed controller were demonstrated by comparing its performance with the one of the conventional sliding mode controller, which is based on integer order derivatives. At the end this paper concluded that FOSMC gives the best control specifications compared with the conventional one based on integer order.

Chapter 3

Model of Induction Motor and SVPWM

3.1 Introduction

AC machines are known by their complex windings and geometries, to lend themselves to an analysis taking into account their exact configurations. It is required to develop a model whose behavior is as close as possible to the real model. The modeling of electrical machines is an important stage for the observation and the analysis of different evolutions of its electromechanical quantities on the one hand and on the other hand, for the elaboration of their control mechanism. Different papers have been published to address the model of an induction motor. Papers [23, 24] presents dynamic model of induction motor in dq reference frame for controller modeling. References [3, 6] indicates that modeling of AC motors in rotating reference frame even though simplifies developing of controller in field oriented control it needs more transformations and makes the system slower. The proposed system will use the model of the motor in stationary reference frame and directly apply nonlinear controllers without the need of complex transformations.

To obtain the model of a system, three tasks must be accomplished

- Choose the system.

- Determine its parameters.
- Finally check its validity using simulations.

An induction motor is a singly exited AC machine in the sense that it is supplied from a single AC source. Its stator winding is directly connected to the AC source while the rotor winding receives energy from the stator by means of induction. The mechanical construction of this motor is different from synchronous motor since there is no supply to the rotor. Based on their rotor construction, induction motors can be classified in to: wound rotor type and the other is squirrel cage type. Of the two types of induction motors, cage type is the most widely used because of its simplest construction, high reliability, and low maintenance frequency [25]. They have a wide variety of applications such as blowers, conveyor, cranes, refrigerators, traction and many other industrial applications, because of their high robustness and reliability. In this thesis, the squirrel cage type induction motors are considered.

In this chapter, brief introduction about squirrel cage induction motors is given. Further, the mathematical formulation of the motor in two phase stationary frames is presented. The modeled motor is then validated in MATLAB/SIMULINK.

3.2 Modeling of Squirrel Cage Induction Motor

An asynchronous machine is an AC machine whose rotor speed and the rotating magnetic field speed are not equal. The rotor is always delayed with respect to the speed of the stator field. The asynchronous machine is called induction machine because the energy transferred from the stator to the rotor or vice versa is by electromagnetic induction. The asynchronous machine comprises a fixed part called stator and a rotating part called rotor. It comprises a three-phase winding stator whose magnetic axes are 120 degrees out of phase. The rotor structure can be realized either by a three-phase system with wound rotor or squirrel cage [25]. The schematic representation of the asynchronous machine in the reference (a, b, c) is given in figure 3.1.

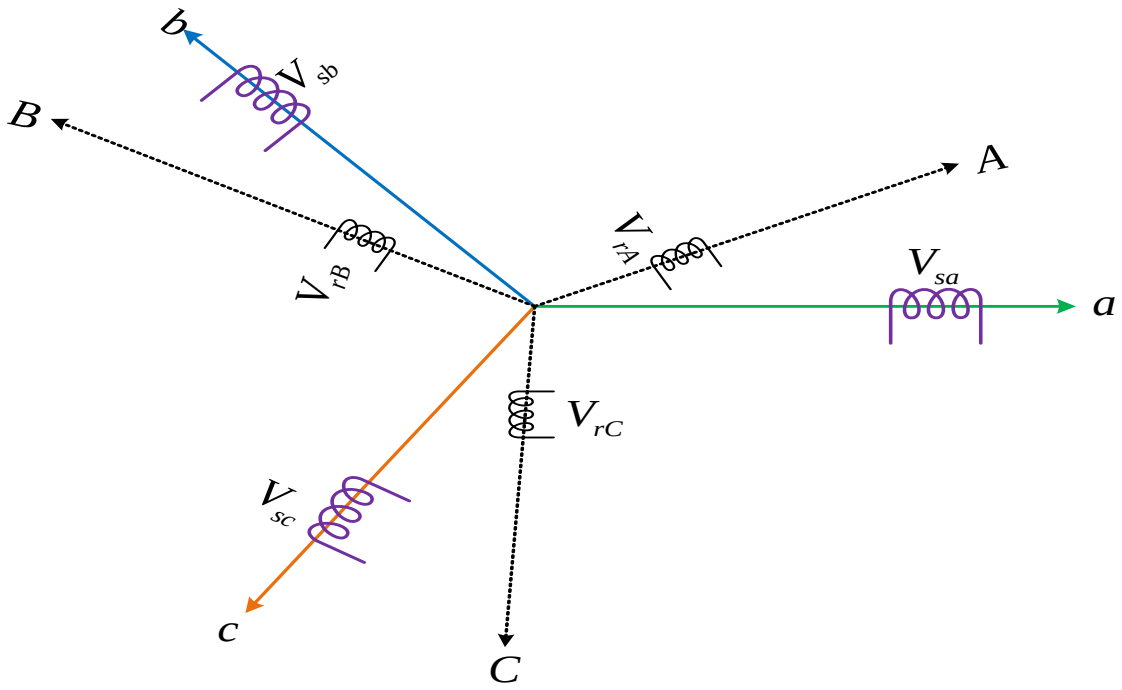

Figure 3.1: Representation of thee phase quantities in ABC frame of reference

In the context by using the following simplifying assumptions:

- The air gap is uniform
- Operation is in the unsaturated region
- Hysteresis, eddy currents and skin effect are neglected
- The winding is symmetrically distributed to give sinusoidal MMF.

The equations of the machine are written as follows [6]:

At the stator:

$$\begin{bmatrix} V_{sa} \\ V_{sb} \\ V_{sc} \end{bmatrix} = R_s \begin{bmatrix} i_{sa} \\ i_{sb} \\ i_{sc} \end{bmatrix} + \frac{d}{dt} \begin{bmatrix} \lambda_{sa} \\ \lambda_{sb} \\ \lambda_{sc} \end{bmatrix} \tag{3.1}$$

At the rotor:

$$\begin{bmatrix} V_{ra} \\ V_{rb} \\ V_{rc} \end{bmatrix} = R_r \begin{bmatrix} i_{ra} \\ i_{rb} \\ i_{rc} \end{bmatrix} + \frac{d}{dt} \begin{bmatrix} \lambda_{ra} \\ \lambda_{rb} \\ \lambda_{rc} \end{bmatrix} \tag{3.2}$$

3.2.1 Clark and Park Transformation

These transformations transform the three phase variables (voltages, currents, and flux) from fixed reference frame (stationary frame) to a rotating frame (synchronous frame) defined by the Clarke and Park transformations. They are used to reduce the complex nature of the differential equations describing AC machines by eliminating time-varying terms [6, 7]. The transformation from a three-phase stationary frame to a two-phase direct-quadrature (d, q) frame is done by Park transformation. This transformation can be decomposed in two transformations. The first one transforms stationary three-phase system variables (a,b,c) to a stationary two-phase system ($\alpha,\ \beta$) which is known as Clarke transformations. The second one transforms those fixed two-phase variables to a rotating two-phase frame (d,q,0). A general representation of the Park transformation is represented diagramatically in Figure 3.2:

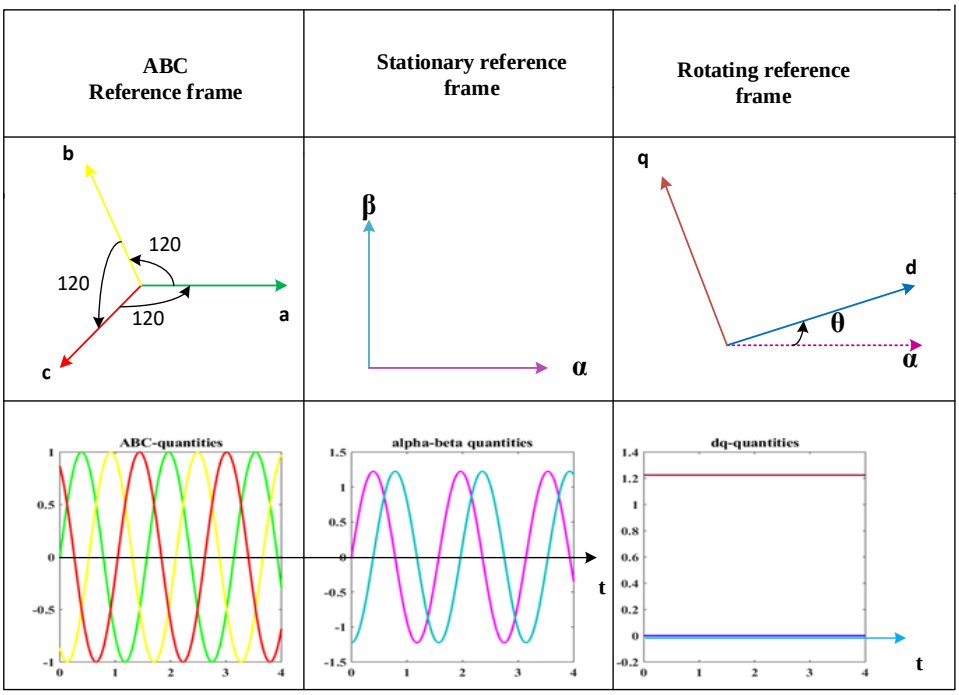

Figure 3.2: Representation of Transformation

The park transformation is done by:

$$\begin{bmatrix} f_\alpha \\ f_\beta \\ f_0 \end{bmatrix} = \sqrt{\frac{2}{3}} \begin{bmatrix} 1 & -\frac{1}{2} & -\frac{1}{2} \\ 0 & \frac{\sqrt{3}}{2} & -\frac{\sqrt{3}}{2} \\ \frac{1}{2} & \frac{1}{2} & \frac{1}{2} \end{bmatrix} \begin{bmatrix} f_a \\ f_b \\ f_c \end{bmatrix} \tag{3.3}$$

The Clark transformation is done by:

$$\begin{bmatrix} f_d \\ f_q \end{bmatrix} = \begin{bmatrix} \cos\theta_{da} & \sin\theta_{da} \\ -\sin\theta_{da} & \cos\theta_{da} \end{bmatrix} \begin{bmatrix} f_\alpha \\ f_\beta \end{bmatrix} \tag{3.4}$$

The reverse process can be done by using the concept of inversion of matrices.

3.2.2 Induction Machine Model in Rotating Reference Frame

The equivalent circuit of the motor in rotating reference frame can be represented as in figure 3.3.

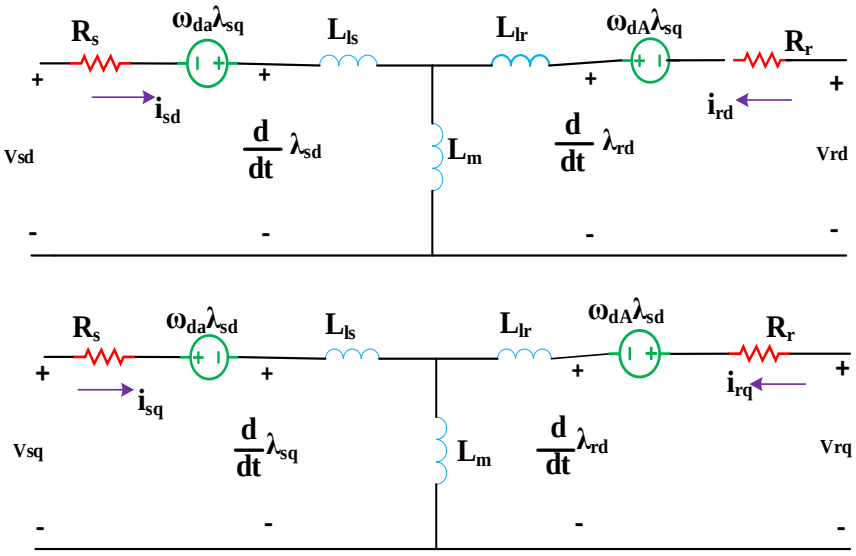

Figure 3.3: Dynamic equivalent circuit of IM

Applying KVL to the stator and rotor side:

$$V_{rq} = R_r i_{rq} + \frac{d\lambda_{rq}}{dt} + \omega_{dA}\lambda_{rd} \tag{3.5}$$

$$V_{sq} = R_s i_{sq} + \frac{d\lambda_{sq}}{dt} + \omega_{da}\lambda_{sd} \tag{3.6}$$

$$V_{rd} = R_r i_{rd} + \frac{d\lambda_{rd}}{dt} - \omega_{dA}\lambda_{rq} \tag{3.7}$$

$$V_{rq} = R_r i_{rq} + \frac{d\lambda_{rq}}{dt} + \omega_{dA}\lambda_{rd} \tag{3.8}$$

$$\omega_{da} = \frac{d\theta_{da}}{dt} \tag{3.9}$$

$$\omega_{dA} = \frac{d\theta_{dA}}{dt} \tag{3.10}$$

As shown in figure 3.4 there are four set of dq windings. The flux linking in any winding is due to the current flowing through it and the current flowing to the other winding on the same axis. This implies that there is no mutual coupling between d and q windings.

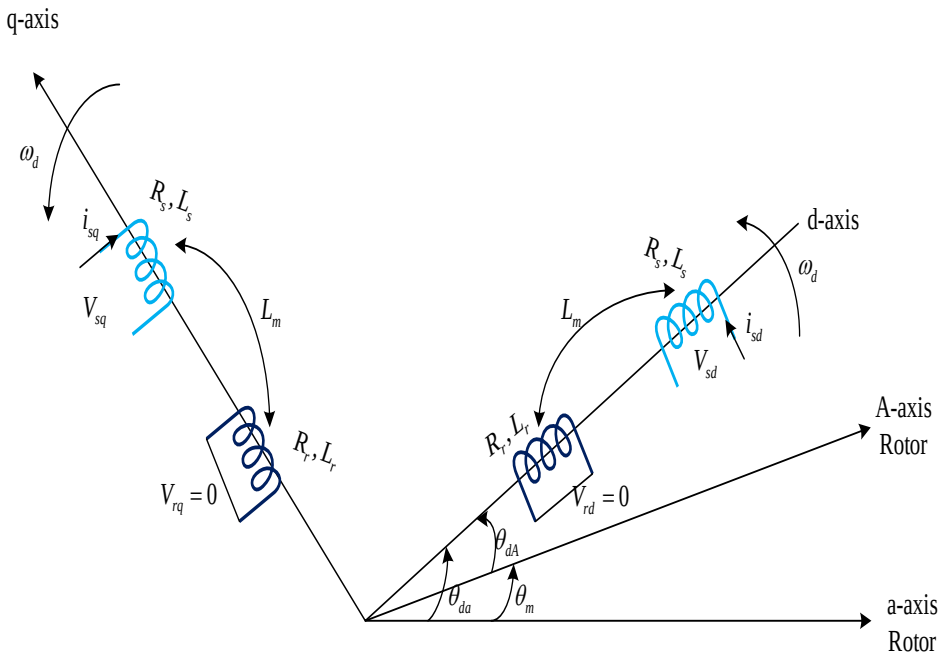

Figure 3.4: Stator and rotor representation by equivalent dq winding currents

Those fluxes can then be expressed as:

$$\lambda_{sd} = L_s i_{sd} + L_m i_{rd} \tag{3.11}$$

$$\lambda_{sq} = L_s i_{sq} + L_m i_{rq} \tag{3.12}$$

$$\lambda_{rd} = L_r i_{rd} + L_m i_{sd} \tag{3.13}$$

$$\lambda_{rq} = L_r i_{rq} + L_m i_{sq} \tag{3.14}$$

Solving for i_{rd} and i_{rq}

$$i_{rd} = \frac{1}{L_r}\lambda_{rd} - \frac{L_m}{L_r}i_{sd} \tag{3.15}$$

$$i_{rq} = \frac{1}{L_r}\lambda_{rq} - \frac{L_m}{L_r}i_{sq} \tag{3.16}$$

$$\frac{d\lambda_{rd}}{dt} = \frac{1}{T_r}\lambda_{rd} - \frac{L_m}{T_r}i_{sd} + \omega_{dA}\lambda_{rq} \tag{3.17}$$

$$\frac{d\lambda_{rq}}{dt} = \frac{1}{T_r}\lambda_{rq} - \frac{L_m}{T_r}i_{sq} - \omega_{dA}\lambda_{rd} \tag{3.18}$$

Now simplifying the above expressions can result rotor flux as a function of stator flux and stator current and on the other hand stator flux in terms of rotor flux and stator current as:

$$\vec{\lambda}_r = \frac{L_r\vec{\lambda}_s - L_sL_r\sigma\overrightarrow{i_s}}{L_m} \tag{3.19}$$

$$\vec{\lambda}_s = \frac{L_m\vec{\lambda}_r + L_sL_r\sigma\overrightarrow{i_s}}{L_r} \tag{3.20}$$

$$\begin{cases} \frac{di_{sd}}{dt} = \frac{1}{\sigma L_s}\left(-\left(R_s + \frac{L_m^2}{L_rT_r}\right)i_{sd} + \omega_{da}\sigma L_s i_{sq} + \frac{L_m}{L_rT_r}\lambda_{rd} + \frac{L_m}{L_r}\omega_m\lambda_{rq} + V_{sd}\right) \\ \frac{di_{sq}}{dt} = \frac{1}{\sigma L_s}\left(-\omega_{da}\sigma L_s i_{sd} - \left(R_s + \frac{L_m^2}{L_rT_r}\right)i_{sq} - \frac{L_m}{L_r}\omega_m\lambda_{rd} + \frac{L_m}{L_rT_r}\lambda_{rq} + V_{sq}\right) \\ \frac{d\lambda_{rd}}{dt} = \frac{L_m}{L_r}i_{sd} - \frac{1}{T_r}\lambda_{rd} + \omega_{dA}\lambda_{rq} \\ \frac{d\lambda_{rq}}{dt} = \frac{L_m}{L_r}i_{sq} - \omega_{dA}\lambda_{rd} - \frac{1}{T_r}\lambda_{rq} \end{cases} \tag{3.21}$$

Where $\sigma = 1 - \frac{L_m^2}{L_sL_r}$, $\tau_r = \frac{R_r}{L_r}$, $\omega_m = \omega_{da} - \omega_{dA}$, $\omega_m = \frac{p}{2}\omega_{mech}$

The non-linearity of the model is introduced mainly by the product of angular velocity of the rotor with the components of the flux as well as by the expression of the electromagnetic torque. A much more complete model also takes into account the variations of rotor (stator) resistance and load torque.

3.2.3 Induction Machine Model in Stationary Reference Frame

The second model of the machine is expressed in the reference (α β) frame related to the stator. This model is obtained using the concept of (d q) $\rightarrow$ (α β) transformation and assuming $\omega_{da} = 0$ in the model equation 3.21 [3]. In these conditions the model

will be written as:

$$\begin{cases} \frac{di_{s\alpha}}{dt} = -\gamma i_{s\alpha} + \alpha\beta\lambda_{r\alpha} + \beta\omega_m\lambda_{r\beta} + \frac{V_{s\alpha}}{\sigma} \\ \frac{di_{s\beta}}{dt} = -\gamma i_{s\beta} - \beta\omega_m\lambda_{r\alpha} + \alpha\beta\lambda_{r\beta} + \frac{V_{s\beta}}{\sigma} \\ \frac{d\lambda_{r\alpha}}{dt} = \alpha L_m i_{s\alpha} - \alpha\lambda_{r\alpha} - \omega_m\lambda_{r\beta} \\ \frac{d\lambda_{r\beta}}{dt} = \alpha L_m i_{s\beta} + \omega_m\lambda_{r\alpha} - \alpha\lambda_{r\beta} \end{cases} \tag{3.22}$$

Developed electromagnetic torque

$$T_{em} = p\left(\lambda_{s\alpha} i_{s\beta} - \lambda_{s\beta} i_{s\alpha}\right) = \frac{pL_m}{L_r}\left(\lambda_{r\alpha} i_{s\beta} - \lambda_{r\beta} i_{s\alpha}\right) \tag{3.23}$$

Speed can also be computed using the following dynamics

$$J_{eq}\frac{d\omega_{mech}}{dt} = T_{em} - T_L - f_r\omega_{mech} \tag{3.24}$$

$$\omega_{mech} = \frac{2}{P}\omega_m \tag{3.25}$$

$$\frac{d\omega_m}{dt} = \frac{p}{J_{eq}}(T_{em} - T_L) - \frac{f_r}{J_{eq}}\omega_m \tag{3.26}$$

Now using the following notations:

$$\mu = \frac{p^2 L_m}{J_{eq} L_r} \qquad \sigma = L_s\left(1 - \frac{L_m^2}{L_s L_r}\right) \qquad \beta = \frac{L_m}{\sigma L_r} \qquad k_l = \frac{p}{J_{eq}}$$

$$\alpha = \frac{R_r}{L_r} \qquad \rho = \frac{\mu}{k_l} \qquad \gamma = \frac{R_s}{\sigma} + \alpha\beta L_m \qquad k_f = \frac{f_r}{J_{eq}}$$

The model derived above can be generalized as follows:

$$\begin{cases} \frac{di_{s\alpha}}{dt} = -\gamma i_{s\alpha} + \alpha\beta\lambda_{r\alpha} + \beta\omega_m\lambda_{r\beta} + \frac{V_{s\alpha}}{\sigma} \\ \frac{di_{s\beta}}{dt} = -\gamma i_{s\beta} - \beta\omega_m\lambda_{r\alpha} + \alpha\beta\lambda_{r\beta} + \frac{V_{s\beta}}{\sigma} \\ \frac{d\lambda_{r\alpha}}{dt} = \alpha L_m i_{s\alpha} - \alpha\lambda_{r\alpha} - \omega_m\lambda_{r\beta} \\ \frac{d\lambda_{r\beta}}{dt} = \alpha L_m i_{s\beta} + \omega_m\lambda_{r\alpha} - \alpha\lambda_{r\beta} \\ \frac{d\omega_m}{dt} = \mu\left(\lambda_{r\alpha} i_{s\beta} - \lambda_{r\beta} i_{s\alpha}\right) - k_l T_l - k_f\omega_m \end{cases} \tag{3.27}$$

To test validation of the above designed model, parameters of the machine are essential. Among the various techniques applied to get the parameters of squirrel cage induction motor performing no-load and locked rotor test are most commonly used. A step by step parameter determination of three phase squirrel cage induction motor using experimental designs of no-load test and locked rotor test is presented in [26]. A $3-\phi$, 2 pole, 50 Hz, 1.5 Kw, 230/400 V, 1400 rpm squirrel cage induction motor with parameters determined in [26] presented in table A.1 is used in this thesis to test the validation of all the models.

3.3 Space Vector Pulse Width Modulation (SVPWM) Inverter

To control induction motor drive, it is the most popular way to power the motor with VSI driven by SVPWM. The concept of the SVPWM relies on the representation of the inverter output as space vectors or space phasors. Space vector representation of the output voltages of the inverter is realized for the implementation of SVPWM. Space vector simultaneously represents three-phase quantities as one rotating vector, hence each phase is not considered separately. As its name implies, SVPWM uses the concept of space vector and its geometrical characteristics to derive the on-off time duration of each switch. The objective of the SVPWM control of the inverter switches is to synthesize the desired reference stator voltage space vector in an optimum manner with the following objectives [27]:

- A constant switching frequency fs
- Smallest instantaneous deviation from its reference value
- Maximum utilization of the available dc-bus voltages
- Lowest ripple in the motor current, and
- Minimum switching loss in the inverter.

To implement SVPWM for the two-level VSI it is usually convenient to follow the following procedures [28].

Step1: Find the reference voltage and its angle

A reference voltage vector $\overrightarrow{V}_{sref}$ that rotates with angular speed ω_{da} in the α, β plane represents three sinusoidal waveforms in the abc coordinate system.

Space vector is defined as follows in positive sequence as:

$$F_s = \frac{2}{3}\left(f_a + f_b e^{j\frac{2\pi}{3}} + f_c e^{j\frac{4\pi}{3}}\right) \tag{3.28}$$

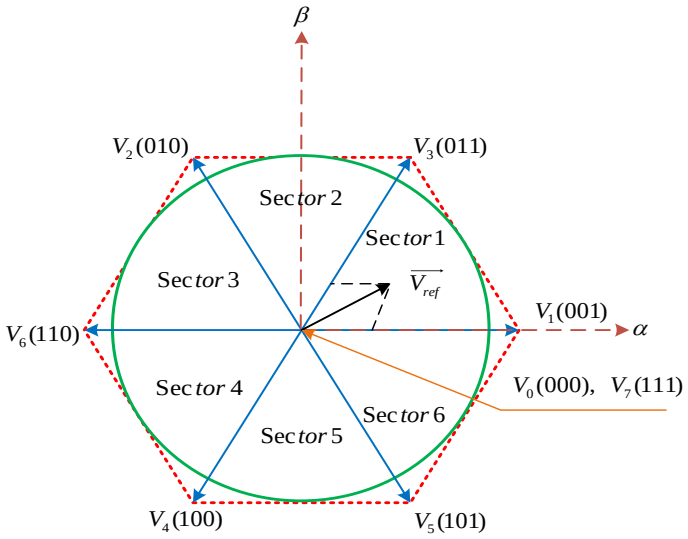

Figure 3.5: Voltage space vector locations corresponding to different switching states

For two-level inverter, the switching vectors are divided into six sectors forming diagram of a hexagon each one can be extended by 60^0. Space vector voltage expression for each sector can be summarized in the Tabel 3.1

Table 3.1: Space vector for a three-phase voltage source inverter

Switching states	**Vector notation**	**Voltage space vectorExpression**
000	$\overrightarrow{V_0}$	0
001	$\overrightarrow{V_1}$	$\frac{2}{3}V_{dc}e^{j0}$
010	$\overrightarrow{V_2}$	$\frac{2}{3}V_{dc}e^{j\frac{2\pi}{3}}$
011	$\overrightarrow{V_3}$	$\frac{2}{3}V_{dc}e^{j\frac{\pi}{3}}$
100	$\overrightarrow{V_4}$	$\frac{2}{3}V_{dc}e^{j\frac{4\pi}{3}}$
101	$\overrightarrow{V_5}$	$\frac{2}{3}V_{dc}e^{j\frac{5\pi}{3}}$
100	$\overrightarrow{V_6}$	$\frac{2}{3}V_{dc}e^{j\frac{\pi}{3}}$
111	$\overrightarrow{V_7}$	0

Figure 3.6 represents basic vectors in one sector from which the reference voltage and its angle as can be obtained follows:

$$|V_{sref}| = \sqrt{{V_{s\alpha}}^2 + {V_{s\beta}}^2} \tag{3.29}$$

$$\alpha = t\,a\,n^{-1}\left(\frac{V_{s\beta}}{V_{s\alpha}}\right) \tag{3.30}$$

Where α is in $\left[-180^0,\ 180^0\right]$

Step 2: Sector identification

After determining the angle, the next step is to locate it in one of the six sectors.

Table 3.2: Sector determination

Sector	Degree included
1	$0^0 \leq \alpha < 60^0$
2	$60^0 \leq \alpha < 120^0$
3	$120^0 \leq \alpha < 180^0$
4	$-180^0 < \alpha < -120^0$
5	$-120^0 \leq \alpha < -60^0$
6	$-60^0 \leq \alpha < 0^0$

Step 3: Dwell time calculation

In this step, the time of application of different space vectors are calculated using "equal volt-second principle". According to this principle, the product of the reference voltage and the sampling/switching time T_s must be equal to the product of the applied voltage vectors and their time of applications.

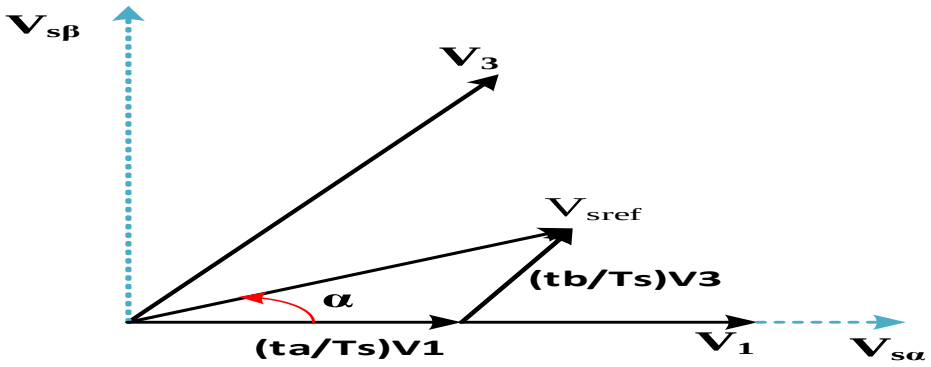

Figure 3.6: Representation of reference vector with two basic vectors

The switching patterns showing the leg voltages in one switching period is depicted in figure 3.7 for sector one. The following analysis will focus on determination of average voltage vector in sector 1 and a generalized discussion will be made to all

sectors. In sector 1 from geometry of figure 3.6 the reference voltage vector can be synthesized by using vectors $\overrightarrow{V}_1$, $\overrightarrow{V}_2$ and $\overrightarrow{V}_0$ (zero vector), applied for time t_a , t_b and t_0 respectively. Hence, using the equal volt-second principle, for sector1:

$$T_s\overrightarrow{V_s^a} = t_a\overrightarrow{V_1} + t_b\overrightarrow{V_3} + t_0\overrightarrow{V_0} \tag{3.31}$$

where $t_a + t_b + t_0 = T_s$ Substituting the values for $\overrightarrow{V_1}$,$\overrightarrow{V_2}$ and $\overrightarrow{V_0}$ from table 3.2:

$$T_s\left|V_{sref}\right|e^{j\alpha} = t_a\frac{2}{3}V_{dc}e^{j0} + t_b\frac{2}{3}V_{dc}e^{j\frac{\pi}{3}} + t_0.0 \tag{3.32}$$

$$T_s\left(V_{s\alpha} + jV_{s\beta}\right) = \frac{2}{3}t_aV_{dc} + \frac{2}{3}t_bV_{dc}cos(\frac{\pi}{3}) + j\frac{2}{3}t_bV_{dc}\ sin(\frac{\pi}{3}) \tag{3.33}$$

$$T_s\left(V_{s\alpha} + jV_{s\beta}\right) = \frac{2}{3}t_aV_{dc} + \frac{2}{3}t_bV_{dc}cos(\frac{\pi}{3}) + j\frac{2}{3}t_bV_{dc}\ sin(\frac{\pi}{3}) \tag{3.34}$$

Equating the real and imaginary parts:

$$t_b = \frac{\sqrt{3}T_sV_{s\beta}}{V_{dc}}, \quad t_a = \frac{\sqrt{3}T_s}{2V_{dc}}\left(\sqrt{3}V_{s\alpha} - V_{s\beta}\right), \quad t_0 = T_s - t_a - t_b \tag{3.35}$$

Following the same procedures for all sectors, obtained results are presented in table 3.3

Table 3.3: Dwell time for each sector

Sector	α	t_a	t_b
1	$0^0 \leq \alpha < 60^0$	$\frac{\sqrt{3}T_s}{2V_{dc}}\left(\sqrt{3}V_{s\alpha} - V_{s\beta}\right)$	$\frac{\sqrt{3}T_s}{V_{dc}}V_{s\beta}$
2	$60^0 \leq \alpha < 120^0$	$-\frac{\sqrt{3}T_s}{2V_{dc}}\left(\sqrt{3}V_{s\alpha} - V_{s\beta}\right)$	$\frac{\sqrt{3}T_s}{2V_{dc}}\left(\sqrt{3}V_{s\alpha} + V_{s\beta}\right)$
3	$120^0 \leq \alpha < 180^0$	$\frac{\sqrt{3}T_s}{V_{dc}}V_{s\beta}$	$-\frac{\sqrt{3}T_s}{2V_{dc}}\left(\sqrt{3}V_{s\alpha} + V_{s\beta}\right)$
4	$-180^0 < \alpha < -120^0$	$-\frac{\sqrt{3}T_s}{V_{dc}}V_{s\beta}$	$-\frac{\sqrt{3}T_s}{2V_{dc}}\left(\sqrt{3}V_{s\alpha} - V_{s\beta}\right)$
5	$-120^0 < \alpha < -60^0$	$-\frac{\sqrt{3}T_s}{2V_{dc}}\left(\sqrt{3}V_{s\alpha} + V_{s\beta}\right)$	$\frac{\sqrt{3}T_s}{2V_{dc}}\left(\sqrt{3}V_{s\alpha} - V_{s\beta}\right)$
6	$-60^0 \leq \alpha < 0^0$	$\frac{\sqrt{3}T_s}{2V_{dc}}\left(\sqrt{3}V_{s\alpha} + V_{s\beta}\right)$	$-\frac{\sqrt{3}T_s}{V_{dc}}V_{s\beta}$

Step 4: Switching Time Duty Cycle

In order to obtain constant switching frequency and optimal harmonic reduction from SVPWM, the average voltage vector should be synthesized by means of the two basic nonzero voltage vectors that form the sector (in which the average voltage vector to be synthesized lies) and both the zero voltage vectors, such that each transition causes change of only one switch status in order to minimize the inverter switching loss.

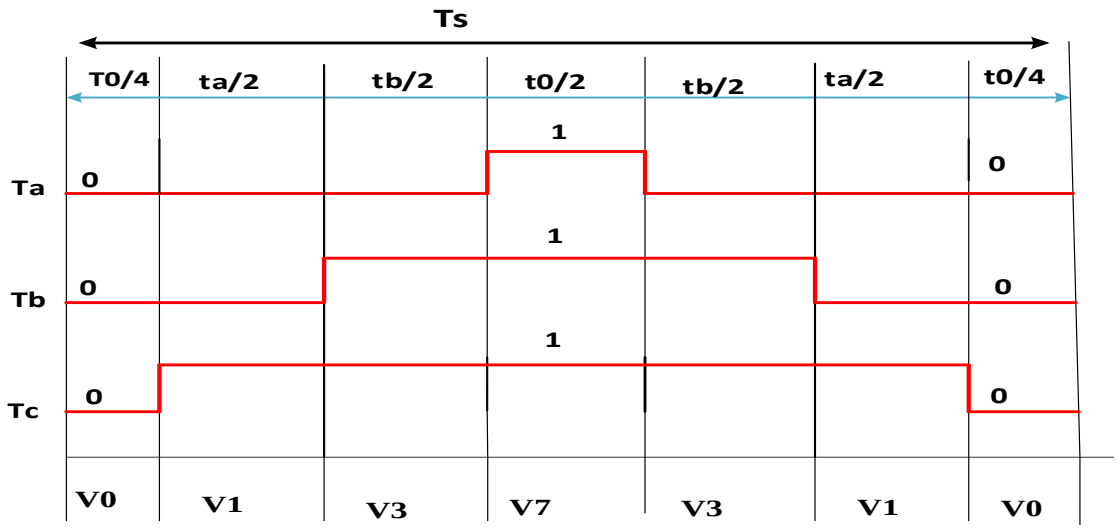

Figure 3.7: Switching pattern for SVPWM for sector 1

Following the same pattern as in figure 3.7 for each sector one can draw an ON/OFF waveform of each phase in each sector. Each switch has its own switching information depending on the location of the reference vector. For Sector 1 for example, the switch T_a is ON for $t_0/4$, T_b is ON for $T_{bon} = t_b/2 + T_{aon}$, and T_c is ON for $t_a/2 + t_b/2 + t_0/4$. Now summarized duty cycles for each sector is presented in table 3.4 below by denoting:

$T_{aon} = t_0/4$, $T_{bon} = t_b/2 + T_{aon}$, $T_{con} = t_a/2 + T_{bon}$

Table 3.4: Switching duty times for each sector

		Sector					
Switch	Duty cycle	1	2	3	4	5	6
Ta	Tda	$Taon$	$Tbon$	$Tcon$	$Tcon$	$Tbon$	$Taon$
Tb	Tdb	$Tbon$	$Taon$	$Taon$	$Tbon$	$Tcon$	$Tcon$
Tc	Tdc	$Tcon$	$Tcon$	$Tbon$	$Taon$	$Taon$	$Tbon$

Step 5: PWM generation

For the switch to know when it should be switched ON at these specific times requires a timer that can give this information. This can be done by modulating those duty cycles with something like a ramp or a repeated sequence having the frequency equal to switching frequency of the devices. Figure 3.8 presents the steps followed in SVPWM.

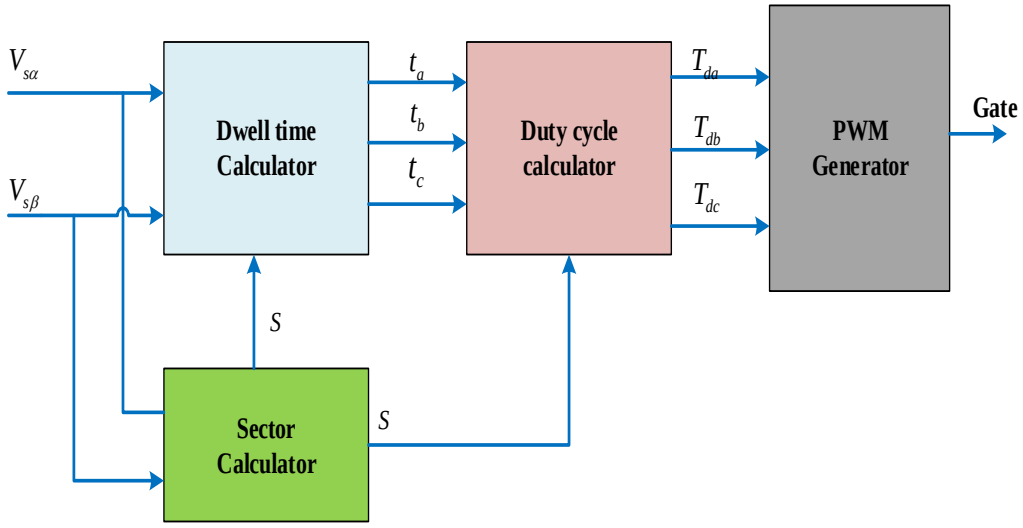

Figure 3.8: Space vector pulse width modulator

Finally, those pulse gates obtained from the SVPWM is used to control the two-level inverter of figure below.

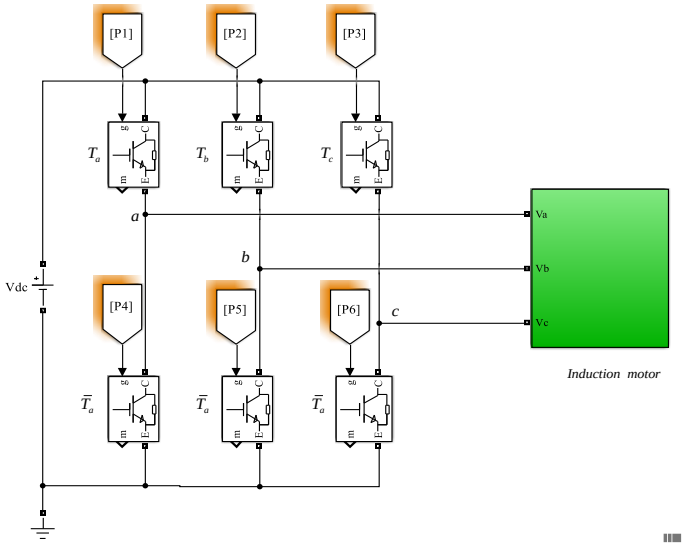

Figure 3.9: Diagram of a three-phase inverter and its load

The output of each phase leg is V_{ao} , V_{bo} and V_{co} for phase A, B and C respectively. Next, equations for phase voltages V_{an} , V_{bn} and V_{cn} which are going to be fed to the motor as is explained in [29].

Line voltages

$$\begin{cases} V_{ab} = V_{b0} - V_{a0} \\ V_{bc} = V_{c0} - V_{b0} \\ V_{ca} = V_{a0} - V_{c0} \end{cases} \tag{3.36}$$

Phase Voltages

$$\begin{cases} V_{an} = \frac{2}{3}V_{a0} - \frac{1}{3}V_{b0} - \frac{1}{3}V_{c0} = \frac{1}{3}\left(V_{ca} - V_{ab}\right) \\ V_{bn} = \frac{2}{3}V_{b0} - \frac{1}{3}V_{a0} - \frac{1}{3}V_{c0} = \frac{1}{3}\left(V_{ab} - V_{bc}\right) \\ V_{cn} = \frac{2}{3}V_{c0} - \frac{1}{3}V_{a0} - \frac{1}{3}V_{b0} = \frac{1}{3}\left(V_{bc} - V_{ca}\right) \end{cases} \tag{3.37}$$

The output voltage from the voltage source inverter can be predicted from its DC input and three SVPWM signals using the following formulas.

$$\overrightarrow{V_s^d} = \frac{2}{3}V_{dc}\left(p_a e^{j\pi 0} + p_b e^{j\frac{2}{3}\pi} + p_c e^{j\frac{4}{3}\pi}\right) \tag{3.38}$$

Computing the real part for each voltage component as:

$$\begin{cases} V_a = \frac{2}{3} R\, e \left\{ \overrightarrow{V_s^a} < 0^0 \right\} \\ V_b = \frac{2}{3} R\, e \left\{ \overrightarrow{V_s^a} < -\frac{2\pi}{3} \right\} \\ V_c = \frac{2}{3} R\, e \left\{ \overrightarrow{V_s^a} < \frac{2\pi}{3} \right\} \end{cases} \tag{3.39}$$

Simplifying Equation 3.39 for V_a , V_b and V_c the following can be obtained:

$$\begin{cases} V_a = \frac{V_{dc}}{3} (2p_a - p_b - p_c) \\ V_b = \frac{V_{dc}}{3} (2p_b - p_a - p_c) \\ V_c = \frac{V_{dc}}{3} (2p_c - p_b - p_a) \end{cases} \tag{3.40}$$

3.4 Open Loop Simulation of IM Model

To test whether the derived model is correct or not simulation of motor model using MATLAB/SIMULINK environment and compared results to the expected conceptual results from journals and books to assure if the correct model is obtained. By using motor parameters from table A.1, numerical simulations of a three-phase Squirrel cage motor fed directly by a standard source of RMS value 220V and frequency 50Hz can be studied to know the open loop responses. In the simulation, plots presented in the first step, no load operation of the machine is numerically simulated using MATLAB 2017B and generated plots are presented in figure 3.11. Examination of curves in 3.11e shows that at the first moments of startup, stator current has successive oscillations, and quickly disappear in steady state to give rise to a sinusoidal shape of constant amplitude. The rotor flux trajectories in (α β) plane is also presented in 3.11i for no load case and in 3.11j for loaded case. As can be seen from 3.11c, the speed increase is almost linear at the starting and then stabilizes in steady state at the speed close to that of synchronous speed. It can also be observed that the rotor flux circular trajectory seems to follow a random path in unloaded condition. In the second step, a disturbance of the load torque presented in figure 3.11b is introduced to the motor shaft and simulation results for rotor speed in 3.11d, stator currents in

3.11f, rotor flux in 3.11h and developed electromagnetic torque are presented. When load is applied, the electromagnetic torque reaches its reference value to compensate for this load with an almost instantaneous response before stabilizing at the applied load torque value with some oscillations during instantaneous changes of load torque. A permanent decrease of the speed appears until applied load is removed, this is due to the fact that there is no controller that can counter act for this unexpected disturbance. The stator currents change permanently according to the load applied to the motor shaft. The rotor flux circular trajectory as can be observed follows a more random path than the unloaded trajectory.

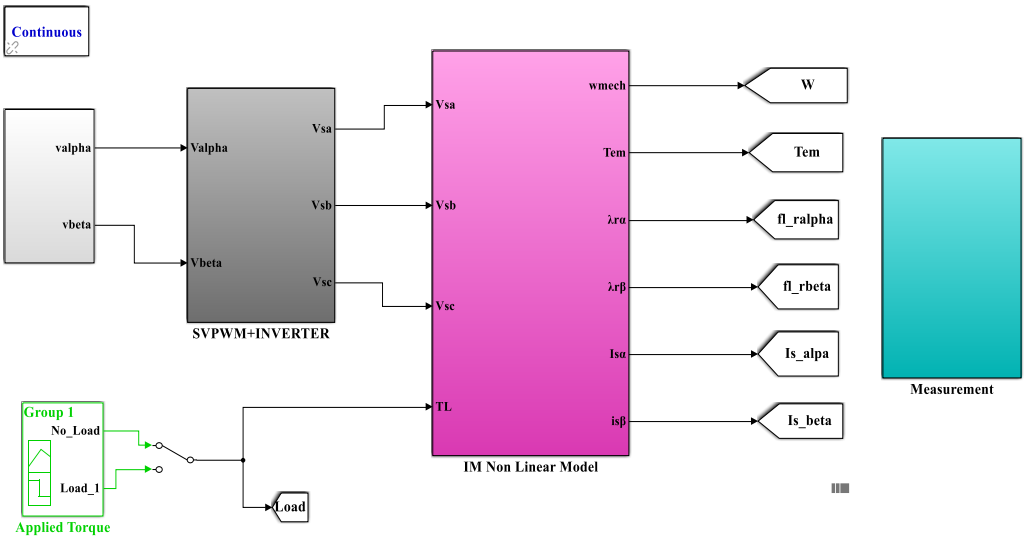

Figure 3.10: Model of squirrel cage motor in stationary frame

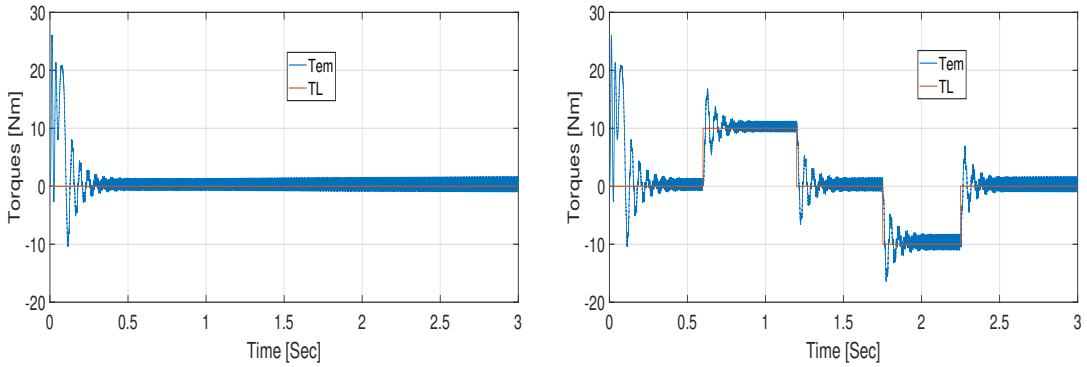

(a) (b)

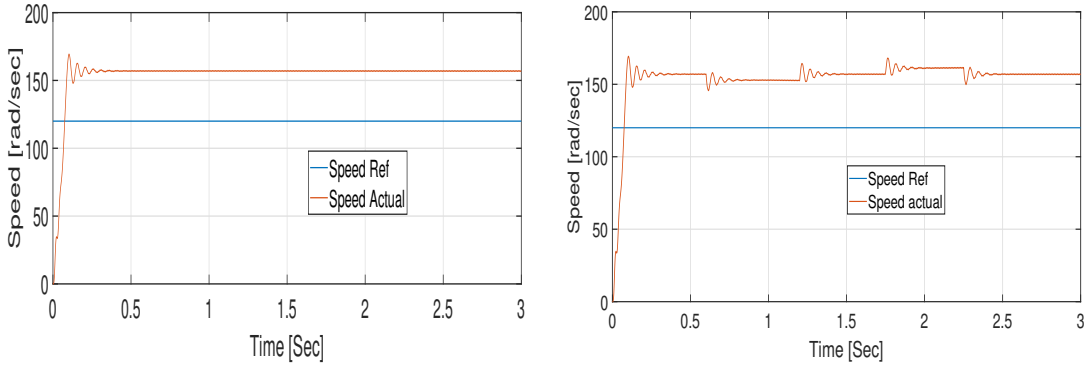

(c)

(d)

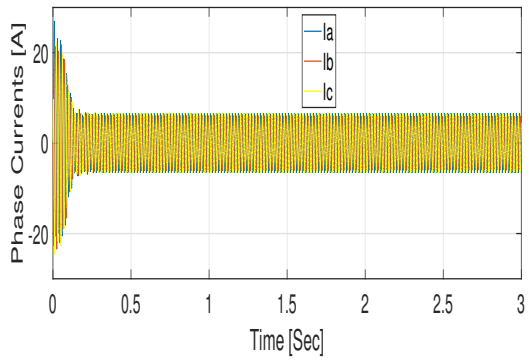

(e)

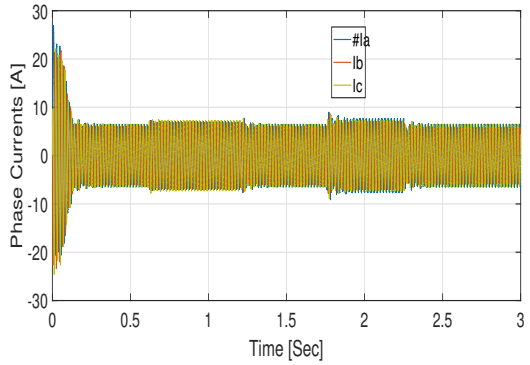

(f)

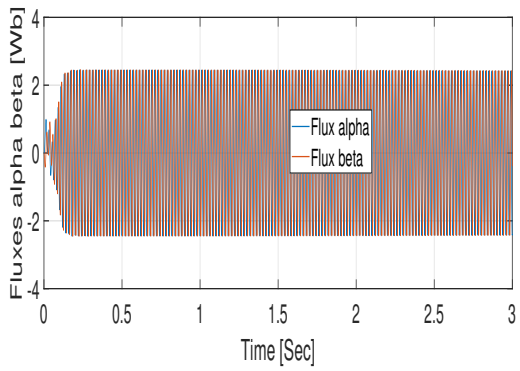

(g)

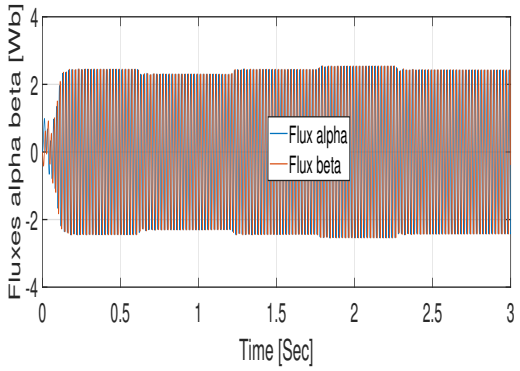

(h)

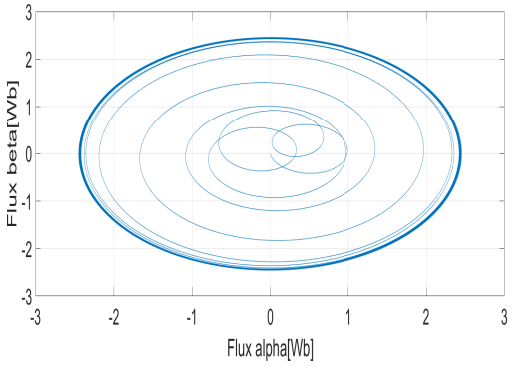

(i)

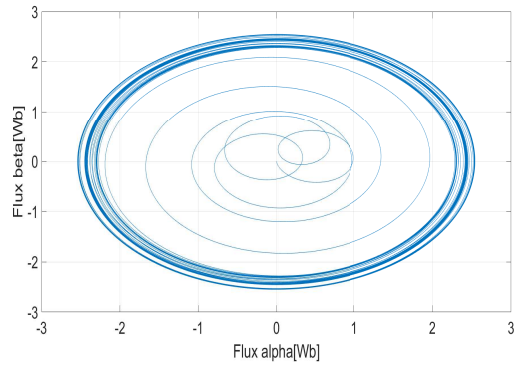

(j)

Figure 3.11: Open loop simulations results

Chapter 4

Modeling of Controller and Estimator

The application of vector control allows an effective decoupling between the flux of the induction machine and its electromagnetic torque. However, load variation or parameter variations lead to loss of decoupling. To overcome these difficulties, several control strategies are proposed in literatures among the control strategies offering high dynamic performance, there is the non-linear control, called control by input-output linearization [30]. The purpose of this technique is to compensate for nonlinearities present in the machine and, therefore, ensure a perfect decoupling between flux and torque. The following section focusses on the application of nonlinear controller to squirrel cage induction machine supposing that all states are measurable and model of nonlinear IOFL is developed.

4.1 The concept of IOFL

Feedback linearization is an approach to nonlinear control system which has attracted a great deal of research interest in recent years. Feedback linearization techniques can be viewed as ways of transforming original system models into equivalent models of a simpler form.

Let us consider the nonlinear system whose general representation is given as [31, 32]:

$$\begin{cases} \dot{x} = f(x) + g(x)\,u \\ y = h(x) \end{cases} \tag{4.1}$$

Taking the first derivative of y the following can be obtained:

$$\dot{y} = \frac{\partial h(x)}{\partial x}\,\dot{x} = \frac{\partial h(x)}{\partial x}\,[f(x) + g(x)\,u] = L_f h(x) + L_g h(x)\,u \tag{4.2}$$

If $L_g h(x) = 0$, differentiating is continued until the inputs appear in the r^{th} derivative of output. Generalized expression is then:

$$y^r = L_f^r h(x) + L_g L_f^{r-1} h(x)\,u \tag{4.3}$$

Where the following are notations used in this context

$$L_f h(x) = \frac{\partial h}{\partial x} f(x) \qquad L_f^2 h(x) = \frac{\partial (L_f h)}{\partial x} f(x)$$

$$L_g h(x) = \frac{\partial h}{\partial x} g(x) \qquad L_f^0 h(x) = h(x)$$

$$L_g L_f h(x) = \frac{\partial (L_f h)}{\partial x} g(x) \qquad L_f^k h(x) = L_f L_f^{k-1} h(x) = \frac{\partial (L_f^{k-1} h)}{\partial x} f(x)$$

When u does not appear in y, $\dot{y}$, ..., y^{r-1} and appears in equation of y^r with a non-zero coefficient, the system is input output feedback linearizable and state feedback control is:

$$u = \frac{1}{L_g L_f^{r-1} h(x)} [v - L_f^r h(x)] \tag{4.4}$$

Where $v = y^r$ and r is called the relative degree of the system. To ensure perfect tracking and to get the required behavior, auxiliary inputs can be defined as:

$$V_i = y_{iref}^{r_i} - k_1 e - k_2 e' - ... - k_r e^{r-1}, \qquad Where \qquad e = y_i - y_{iref} \tag{4.5}$$

In the above equation k_r is a positive coefficient that should be chosen to guarantee the system convergence.

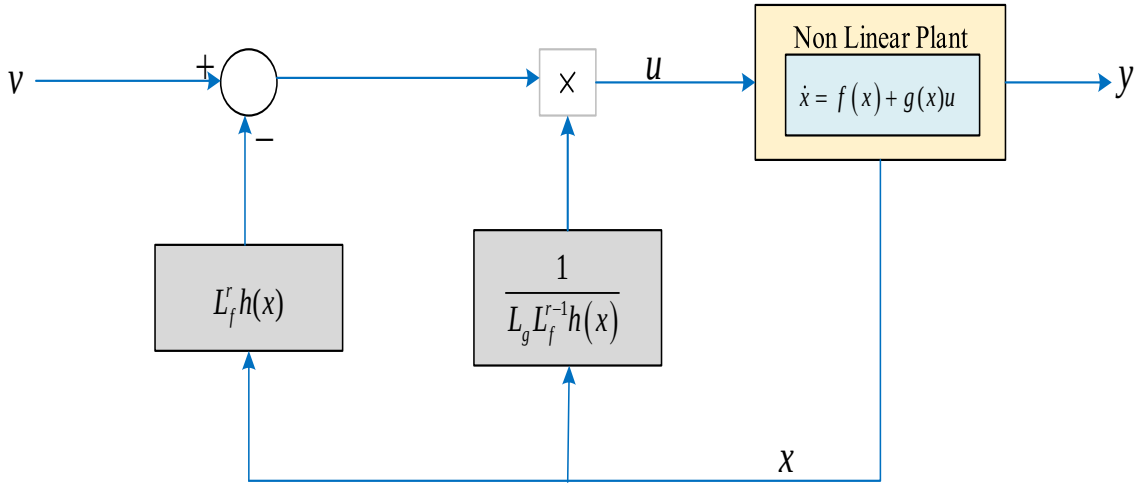

Figure 4.1: General block of input output feedback linearization

Similar procedure can be followed for MIMO systems like induction motor model with little modification. Extending derivation for a system having input and outputs of the form:

$$\begin{cases} \dot{x} = f(x) + \sum_{i=1}^{m} g_i(x)\, u_i \\ y_i = h_i(x), \qquad where \;\; 0 < i \leq m \end{cases} \tag{4.6}$$

Differentiating each output as it was done previously for SISO systems the control law for MIMO system can be obtained as:

$$u = C^{-1} \left(\begin{bmatrix} v_1 \\ . \\ . \\ v_m \end{bmatrix} - \begin{bmatrix} L_f^{r1} h_1(x) \\ . \\ . \\ L_f^{rm} h_m(x) \end{bmatrix} \right) \tag{4.7}$$

$$\text{where } C = \begin{bmatrix} L_{g11}L_f^{r1-1}h_1 & . & . & L_{g1m}L_f^{r-1}h_1 \\ . & . & . & . \\ . & . & . & . \\ L_{g11}L_f^{rm-1}h_m & . & . & L_{g1m}L_f^{rm-1}h_m \end{bmatrix}$$

4.2 Model of IOFL for induction motor

The input-output linearization control is based on the model of induction machine in (α, β) reference frame fixed to stator. Using the above concepts to induction motor system by rearranging the model presented in equation 3.27 to take a form of equation 4.1.

$$f(x) = \begin{bmatrix} -\gamma i_{s\alpha} + \alpha\beta\lambda_{r\alpha} + \beta\omega_m\lambda_{r\beta} \\ -\gamma i_{s\beta} - \beta\omega_m\lambda_{r\alpha} + \alpha\beta\lambda_{r\beta} \\ \alpha L_m i_{s\alpha} - \alpha\lambda_{r\alpha} - \omega_m\lambda_{r\beta} \\ \alpha L_m i_{s\beta} + \omega_m\lambda_{r\alpha} - \alpha\lambda_{r\beta} \\ \mu\left(\lambda_{r\alpha}i_{s\beta} - \lambda_{r\beta}i_{s\alpha}\right) - k_l T_l - k_f\omega_m \end{bmatrix}, \qquad \begin{bmatrix} y_1 \\ y_2 \end{bmatrix} = \begin{bmatrix} T_{em} \\ \lambda_{r\alpha}^2 + \lambda_{r\beta}^2 \end{bmatrix}$$

$$x = [i_{s\alpha} \;\; i_{s\beta} \;\; \lambda_{s\alpha} \;\; \lambda_{s\beta} \;\; \omega_m]^T \qquad u = [V_{s\alpha} \; V_{s\beta}]^T$$

$$g(x) = \begin{bmatrix} \frac{1}{\sigma} & 0 & 0 & 0 & 0 \\ 0 & \frac{1}{\sigma} & 0 & 0 & 0 \end{bmatrix}^T$$

Now proceeding successive derivation of outputs leads to the following:

$$y_1 = T_{em} = \rho\left(\lambda_{r\alpha}i_{s\beta} - \lambda_{r\beta}i_{s\alpha}\right) \tag{4.8}$$

$$y_1' = L_f h(x) = \rho(\lambda_{r\alpha}'i_{s\beta} + \lambda_{r\alpha}i_{s\beta}' - \lambda_{r\beta}'i_{s\alpha} + \lambda_{r\beta}i_{s\alpha}') \tag{4.9}$$

$$\begin{aligned} y_1' = L_f h_1(x) = \rho\left(\alpha+\gamma\right)\left(i_{s\alpha}\lambda_{s\beta} - i_{s\beta}\lambda_{s\alpha}\right) - \rho\omega_m\left(i_{s\alpha}\lambda_{s\alpha} + i_{s\beta}\lambda_{s\beta}\right) \\ -\rho\beta\omega_m\left(\lambda_{r\alpha}^2 + \lambda_{r\beta}^2\right) - \frac{\rho}{\sigma}\lambda_{r\beta}V_{s\alpha} + \frac{\rho}{\sigma}\lambda_{r\alpha}V_{s\beta} \end{aligned} \tag{4.10}$$

$$y_2' = L_f h_2(x) = 2\lambda_{r\alpha}\lambda_{r\alpha}' + 2\lambda_{r\beta}\lambda_{r\beta}' \tag{4.11}$$

$$y_2' = L_f h_2(x) = 2\alpha L_m\left(i_{s\alpha}\lambda_{r\alpha} + i_{s\beta}\lambda_{r\beta}\right) - 2\alpha\left(\lambda_{r\alpha}^2 + \lambda_{r\beta}^2\right) \tag{4.12}$$

$$\begin{aligned} y_2'' = L_f^2 h_2(x) = 2\alpha L_m \left(i'_{s\alpha}\lambda_{r\alpha} + i_{s\alpha}\lambda'_{r\alpha} + i'_{s\beta}\lambda_{r\beta} + i_{s\beta}\lambda'_{r\beta}\right) \\ -4\alpha \left(\lambda_{r\alpha}\lambda'_{r\alpha} + \lambda_{r\beta}\lambda'_{r\beta}\right) \end{aligned} \tag{4.13}$$

$$\begin{aligned} y_2'' = L_f^2 h_2(x) = -2\alpha L_m(\gamma + 3\alpha)\left(i_{s\alpha}\lambda_{r\alpha} + i_{s\beta}\lambda_{r\beta}\right) - 2\alpha L_m \omega_m \left(i_{s\alpha}\lambda_{r\beta} - i_{s\beta}\lambda_{r\alpha}\right) \\ +2\alpha^2(2 + \beta L_m)\left(\lambda_{r\alpha}^2 + \lambda_{r\beta}^2\right) + 2(\alpha L_m)^2\left(i_{s\alpha}^2 + i_{s\beta}^2\right) \\ +\tfrac{2\alpha L_m}{\sigma}\lambda_{r\alpha}V_{s\alpha} + \tfrac{2\alpha L_m}{\sigma}\lambda_{r\beta}V_{s\beta} \end{aligned} \tag{4.14}$$

From the above derivatives it can be seen that relative degrees of torque and flux squared are $r_1 = 1$ and $r_2 = 2$ respectively. Then the sum of the relative degrees of speed and flux is less than degree of the system $r = 5$ implying that some change of variables are required [32].

After understanding those concepts and having the outputs to be controlled T_{em} and $\lambda_{r\alpha}^2 + \lambda_{r\beta}^2$, follows defining change of coordinates to assist the lie derivatives as:

$$\begin{cases} y_1 = h_1(x) = T_{em} = \rho\left(\lambda_{r\alpha}i_{s\beta} - \lambda_{r\beta}i_{s\alpha}\right) \\ y_2 = h_2(x) = \lambda_{r\alpha}^2 + \lambda_{r\beta}^2 \\ y_3 = L_f h_2(x) = 2\alpha L_m\left(i_{s\alpha}\lambda_{r\alpha} + i_{s\beta}\lambda_{r\beta}\right) - 2\alpha\left(\lambda_{r\alpha}^2 + \lambda_{r\beta}^2\right) \\ y_4 = \tan^{-1}(\frac{\lambda_{r\beta}}{\lambda_{r\alpha}}) \\ y_5 = h_3(x) = \omega_m \end{cases} \tag{4.15}$$

Usually the choice of the variable y_4 is arbitrary, this variable represents the position of the rotor flux [30]. Using inverse transformation IM model states in new coordinate can be obtained as:

$$\omega_m = y_5\,,\ \lambda_{r\alpha} = \sqrt{y_2}\,cos\,(\,y_4)\ ,\ \lambda_{r\beta} = \sqrt{y_2}\,sin\,(\,y_4)$$

$$i_{s\alpha} = \frac{1}{\sqrt{y_2}}\left[\frac{cos\,y_4}{2\alpha L_m}\left(y_3 + 2\alpha y_2\right) - \frac{sin\,y_4}{\rho}y_1\right],\ i_{s\beta} = \frac{1}{\sqrt{y_2}}\left[\frac{sin\,y_4}{2\alpha L_m}\left(y_3 + 2\alpha y_2\right) + \frac{cos\,y_4}{\rho}y_1\right]$$

After this change of variables, and using the induction motor states in the new coordinates a control law describing linear relationship between inputs and outputs can

be obtained as the following:

$$\begin{bmatrix} y_1{}' \\ y_2{}'' \end{bmatrix} = \begin{bmatrix} L_f h_1 \\ L_f^2 h_2 \end{bmatrix} + \begin{bmatrix} L_{g_{11}} h_1 & L_{g_{12}} h_1 \\ L_{g_{21}} L_f h_2 & L_{g_{22}} L_f h_2 \end{bmatrix} u \tag{4.16}$$

Where $L_{g_{12}} h_1 = \frac{\rho}{\sigma}\lambda_{r\alpha}$, $L_{g_{11}} h_1 = -\frac{\rho}{\sigma}\lambda_{r\beta}$, $L_{g_{12}} h_1 = \frac{\rho}{\sigma}\lambda_{r\alpha}$, $L_{g_{22}} L_f h_2 = \frac{2\alpha L_m}{\sigma}\lambda_{r\beta}$

$$L_f h_1 = \rho\left(\alpha+\gamma\right)\left(i_{s\alpha}\lambda_{s\beta} - i_{s\beta}\lambda_{s\alpha}\right) - \rho\omega_m\left(i_{s\alpha}\lambda_{s\alpha} + i_{s\beta}\lambda_{s\beta}\right) - \rho\beta\omega_m\left(\lambda_{r\alpha}^2 + \lambda_{r\beta}^2\right)$$

$$\begin{aligned} L_f^2 h_2 = &-2\alpha L_m(\gamma+3\alpha)\left(i_{s\alpha}\lambda_{r\alpha} + i_{s\beta}\lambda_{r\beta}\right) - 2\alpha L_m\omega_m\left(i_{s\alpha}\lambda_{r\beta} - i_{s\beta}\lambda_{r\alpha}\right) \\ &+2\alpha^2(2+\beta L_m)\left(\lambda_{r\alpha}^2 + \lambda_{r\beta}^2\right) + 2(\alpha L_m)^2\left(i_{s\alpha}^2 + i_{s\beta}^2\right) \end{aligned}$$

$$\begin{bmatrix} y_1' \\ y_2'' \end{bmatrix} = \begin{bmatrix} v_\alpha \\ v_\beta \end{bmatrix} = V = F(x) + C(x)u \tag{4.17}$$

$$C(x) = \begin{bmatrix} -\frac{\rho}{\sigma}\lambda_{r\beta} & \frac{\rho}{\sigma}\lambda_{r\alpha} \\ \frac{2\alpha L_m}{\sigma}\lambda_{r\alpha} & \frac{2\alpha L_m}{\sigma}\lambda_{r\beta} \end{bmatrix} \tag{4.18}$$

$C(x)$ is the decoupling matrix whose determinant can be computed as:

$$det[C(x)] = -\frac{2\alpha\rho L_m}{\sigma^2}[\lambda_{r\alpha}^2 + \lambda_{r\beta}^2] \tag{4.19}$$

Note that the decoupling matrix is not singular except at the starting point. This problem can be avoided by choosing nonzero initial conditions when observing of rotor flux.

It can be written in general form:

$$u = C^{-1}(x)[V - F(x)] \tag{4.20}$$

Where $C^{-1}(x) = \frac{1}{det[C(x)]}\begin{bmatrix} \frac{2\alpha L_m}{\sigma}\lambda_{r\beta} & \frac{\rho}{\sigma}\lambda_{r\alpha} \\ \frac{2\alpha L_m}{\sigma}\lambda_{r\alpha} & -\frac{\rho}{\sigma}\lambda_{r\beta} \end{bmatrix}$

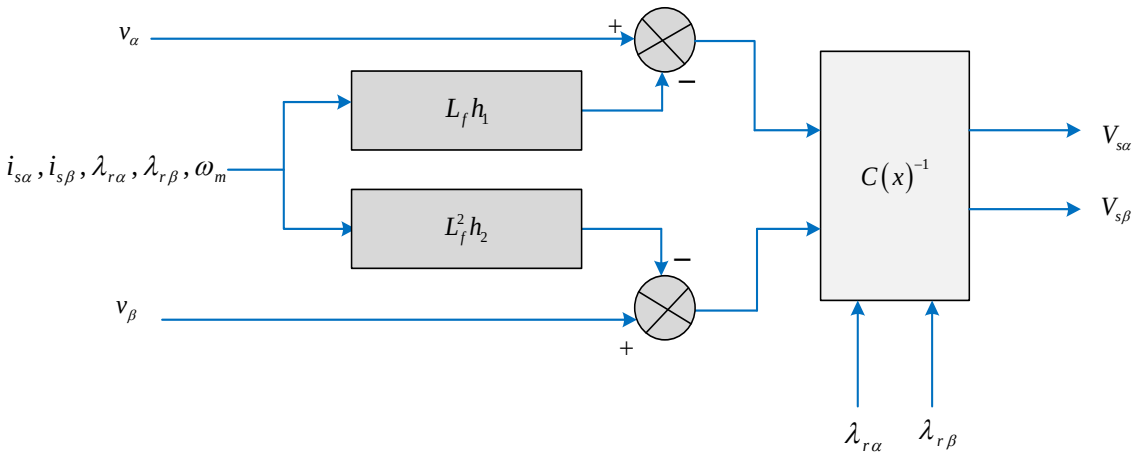

Figure 4.2: Input output feedback linearization of induction motor model

The state feedback defined by the above equation decouples and linearizes the system. Therefore, the system closed loop is equivalent to two chains of two independent integrators:

$$V = \begin{bmatrix} v_\alpha \\ v_\beta \end{bmatrix} = \begin{bmatrix} \dot{y}_1 \\ \ddot{y}_2 \end{bmatrix} \tag{4.21}$$

The vector V represents an external set point of the linearized system. To ensure perfect tracking and to get the required behavior, auxiliary inputs can be defined as: Setting $y_r = [\ T_{em} \quad \lambda_r^2\ ]^T$ as a reference trajectory, the command can be calculated from the following way:

$$\begin{cases} v_\alpha = -k_{a1}(T_{em} - T_{emref}) + T'_{emref} \\ v_\beta = -k_{b1}(\lambda_r^2 - \lambda_{ref}^2) - k_{b2}(\lambda_r^{2'} - \lambda_{ref}^{2'}) + \lambda_r^{2''} \end{cases} \tag{4.22}$$

This choice leads to the dynamics:

$$\begin{cases} \dot{e_1} + k_{a1} e_1 = 0 \\ \ddot{e_2} + k_{b2}\, \dot{e_2} + k_{b1} e_2 = 0 \end{cases} \tag{4.23}$$

Where the tracking errors are defined as $e_1 = T_{em} - T_{emref}, \qquad e_2 = \lambda_r^2 - \lambda_{ref}^2$

The dynamics above will be stable if the polynomials of characteristics equation in e_1 and e_2 have their roots on the left hand side of the complex plane. Under these conditions, it is possible to bring the actual speed to the reference speed and the flux standard to reference flux with imposed dynamics. The control law gains should be chosen to satisfy Lyapunov stability's condition. For this thesis the values of selected gains resulting better tracking response are $k_{a1} = k_{b1} = 8*10^4$ and $k_{b2} = 4*10^3$

4.3 Model of speed controller

4.3.1 PID speed controller

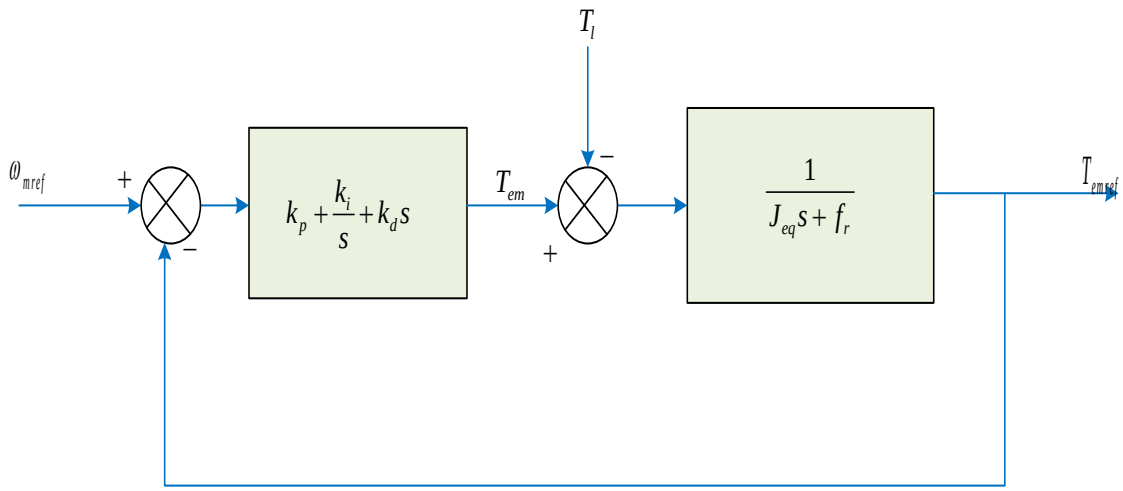

Figure 4.3: Structure of PID Speed controller

Earlier, model of nonlinear controller to independently control electromagnetic torque and flux based on the external references using IOFL is discussed. Flux reference is set by the user but torque reference is obtained from speed controller block. Speed has been controlled using PID controller which is the most popular controller in electrical drives. But, the type of speed controller used really matters.

The governing differential equation for the mechanical system of the motor is expressed as:

$$\frac{d\omega_{mech}}{dt} = \frac{1}{J_{eq}}\left(T_{em} - T_L\right) - \frac{f_r}{J_{eq}}\omega_{mech} \tag{4.24}$$

For the system described by the above dynamics popular PID controller of the form:

$$C\left(e_{\omega m}\right) = k_p e_{\omega m} + \frac{k_i}{s} e_{\omega m} + k_d s e_{\omega m} \tag{4.25}$$

is applied. The gains of PID controllers should be tuned using appropriate tuning mechanism. In this thesis, it is tuned using root locus tuning method as it is clearly discussed in [33] for comparison purpose to the proposed controller.

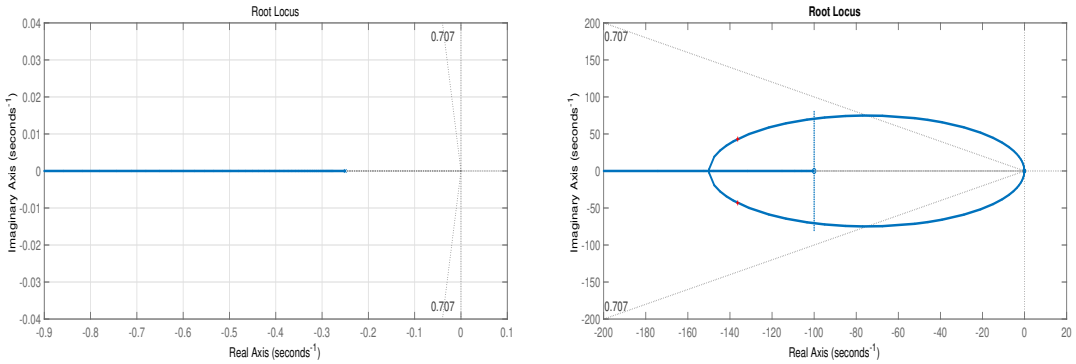

(a) (b)

Figure 4.4: Open loop (a) and closed loop Root locus (b) of the speed loop

The gains of PID speed controllers obtained from this root locus technique and applied for simulation sections later are $k_p = 0.924$, $k_i = 8.4$ and $k_d = 0.0084$.

4.3.2 Sliding Mode Controllers

Sliding mode controller is a well-known controller recognized as a powerful tool to robustly control systems with uncertainties. It does not require exact model of the system since it is robust against parameter uncertainty, external disturbance and modeling error. Application of this controller aims to steer the system state trajectory onto a particular surface in the state space. Sliding mode controller modeling

approach has two parts, the first part involves selection of reaching phase while the second one is concerned about selection of the control law. The application of SMC is briefly presented below.

$$S_{\omega m} = e_{\omega m} + \lambda_1 \int e_{\omega m} dt \tag{4.26}$$

Where $e_{\omega m} = \omega_{mref} - \omega_{mech}$ is the tuning error signal

Having the derivative of this sliding surface and using equation 4.24 for the speed dynamics, the following can be obtained:

$$\begin{aligned} S'_{\omega m} &= e'_{\omega m} + \lambda_1 e_{\omega m} \\ &= \lambda_1 e_{\omega m} + \omega'_{mref} - \omega'_{mech} = \lambda_1 e_{\omega m} + \omega'_{mref} - \tfrac{1}{J_{eq}} T_{em} + \tfrac{1}{J_{eq}} T_L + \tfrac{f_r}{J_{eq}} \omega_{mech} \end{aligned} \tag{4.27}$$

From this and using exponential reaching law the control law can be derived as:

$$S'_{\omega m} = -k_r S_{\omega m} - K_s sign(S_{\omega m}) \tag{4.28}$$

Where

$$sign(S_{\omega m}) = \begin{cases} 1 & S_{\omega m} > 0 \\ 0 & S_{\omega m} = 0 \\ -1 & S_{\omega m} < 0 \end{cases} \tag{4.29}$$

$$\begin{aligned} &\lambda_1 e_{\omega m} + \omega'_{mref} - \tfrac{1}{J_{eq}} T_{em} + \tfrac{1}{J_{eq}} T_L + \tfrac{f_r}{J_{eq}} \omega_{mech} = -k_r S_{\omega m} - K_s sign(S_{\omega m}) \\ &\Rightarrow T_{em} = J_{eq} \left(\lambda_1 e_{\omega m} + \omega'_{mref} + \tfrac{1}{J_{eq}} T_L + \tfrac{f_r}{J_{eq}} \omega_{mech} + k_r S_{\omega m} + K_s sign(S_{\omega m}) \right) \end{aligned} \tag{4.30}$$

The general representation of sliding mode control is:

$$u = u_{eq} + u_{dis} \tag{4.31}$$

4.3.3 Fractional order sliding mode speed controller

In recent decades fractional order calculus is becoming a very interesting topic for system modeling and controller development. Using the sliding surface used above but now with a fractional order integrator the control law can be modeled as follows.

$$\begin{aligned} &S_{\omega m} = e_{\omega m} + \lambda_{10} D_t^{-\alpha} e_{\omega m} \\ &where \quad e_{\omega m} = \omega_{mref} - \omega_{mech} \quad and \;\; 0 < \alpha < 1 \end{aligned} \tag{4.32}$$

α is the fractional order of integration

Taking the time derivatives of the above mathematical representations:

$$\begin{aligned} S_{\omega m}^{'} &= e_{\omega m}^{'} + \lambda_{10} D_t^{1-\alpha} e_{\omega m} \\ &= \left(\omega_{mref}^{'} - \tfrac{1}{J_{eq}} T_{em} + \tfrac{1}{J_{eq}} T_L + \tfrac{f_r}{J_{eq}} \omega_{mech} \right) + \lambda_1 D_t^{1-\alpha} e_{\omega m} \end{aligned} \tag{4.33}$$

Using exponential reaching law

$$S_{\omega m}^{'} = -k_r S_{\omega m} - K_s sign(S_{\omega m}) \tag{4.34}$$

The control law can then be computed as:

$$T_{em} = J_{eq} \left(\omega_{mref}^{'} + \frac{1}{J_{eq}} T_L + \frac{f_r}{J_{eq}} \omega_{mech} + \lambda_1 D_t^{1-\alpha} e_{\omega m} + k_r S_{\omega m} + K_s sign(S_{\omega m}) \right) \tag{4.35}$$

4.3.3.1 Stability Analysis of FOSMC

For stability to be guaranteed the lyapunove candidate function should be negative definite

$$V = \frac{1}{2} {S_{\omega m}}^2 \tag{4.36}$$

$$\begin{aligned} V^{'} &= S_{\omega m} S_{\omega m}^{'} \\ &= S_{\omega m} \left(\omega_{mref}^{'} - \tfrac{1}{J_{eq}} T_{em} + \tfrac{1}{J_{eq}} T_L + \tfrac{f_r}{J_{eq}} \omega_{mech} + \lambda_1 D_t^{1-\alpha} e_{\omega m} + \tfrac{1}{J_{eq}} T_L \right) \end{aligned} \tag{4.37}$$

$$V^{'} = S_{\omega m}\left(-k_r S_{\omega m} - K_s sign(S_{\omega m}) + \frac{1}{J_{eq}} T_L\right) \tag{4.38}$$

This implies that the above equation should be negative for stability and the gains should be selected in a way to guarantee the condition.

$$-k_r {S_{\omega m}}^2 - K_s \left|S_{\omega m}\right| + \frac{1}{J_{eq}} S_{\omega m} T_L < 0 \tag{4.39}$$

In this thesis the gains for SMC and FOSMC are in order to satisfy lyapunove stability condition. Generally in exponential reaching the value of K_s should be large enough to bring trajectories with less steady state error. Here $K_s = 2 * 10^3$, $k_r = 5$ and $\lambda_1 = 0.5$ for both SMC and FOSMC. The fractional order integrator $\alpha = 0.2$ for FOSMC control law.

4.4 Load Torque observer

In sliding mode controllers above one can notice that the T_L term present in the control law expression. But, this mechanical shaft load disturbance is unknown term or it is difficult to determine its value using measurement techniques. This necessitates the formulation of load torque observer that can extract its value from estimates of flux and current values. In this thesis the method used to get load torque estimate of permanent magnet synchronous motor in [34] is applied.

Expression for estimated load torque is:

$$\widehat{T_L} = k_{p1}\left(\widehat{\omega_m} - \omega_m\right) + k_{i1}\int\left(\widehat{\omega_m} - \omega_m\right) dt \tag{4.40}$$

Where

$$\widehat{\omega_m} = \frac{1}{j_{eq}s + f_r}\left(T_{em} - \widehat{T_L}\right) \tag{4.41}$$

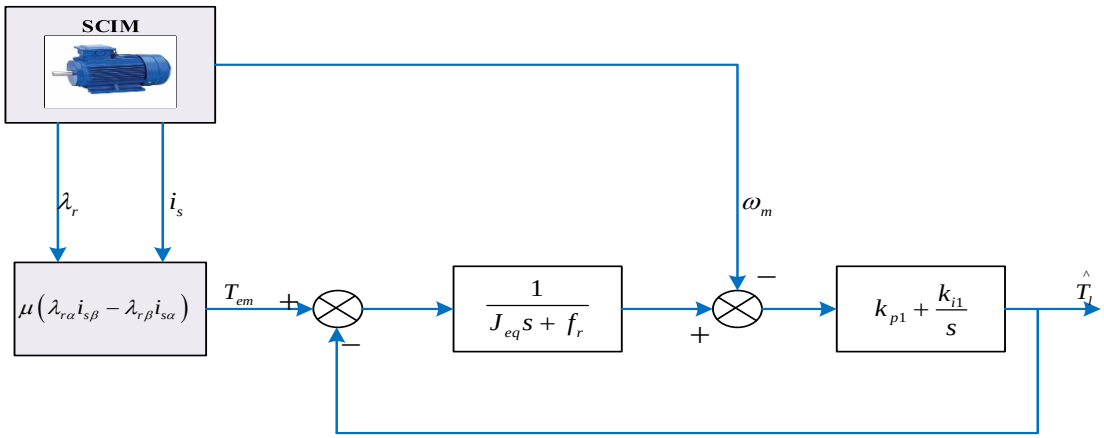

Figure 4.5: Load torque estimator

4.5 Model of Speed Estimator

Input output feedback linearization used above even though gives better results it assumes that all the states are measurable. But, it is difficult to measure some electrical variables for example rotor flux. And also it is better to use estimation algorithm in place of real sensor to measure states in terms of cost minimization of installing the drive system. There for in the following sections, modelling of robust estimation techniques to extract the states of induction motor (rotor flux and speed) more similar to the real measuring device will be discussed. Finally, the validity of choice of the observer will be verified by simulation.

4.5.1 Sliding Mode Rotor Flux Observer

In what follows, sliding-mode observer for the estimation of the rotor flux is studied. Rotor flux is observed through current observer [35]. First, previously derived model of the squirrel cage induction machine expressed in a stationary reference $(\alpha\,\beta)$ is reinterpreted for simplification. Then structure of sliding mode current observer is introduced and then, based on the convergence of this observer, rotor flux will be determined. From the model of IM in $(\alpha\,\beta)$ frame the following representations of

stator current and rotor flux dynamics are obtained:

$$\begin{bmatrix} \frac{di_{s\alpha}}{dt} \\ \frac{di_{s\beta}}{dt} \end{bmatrix} = \beta \left(\begin{bmatrix} \alpha & \omega_m \\ -\omega_m & \alpha \end{bmatrix} \begin{bmatrix} \lambda_{r\alpha} \\ \lambda_{r\beta} \end{bmatrix} - \alpha L_m \begin{bmatrix} i_{s\alpha} \\ i_{s\beta} \end{bmatrix} \right) - \frac{R_s}{\sigma} \begin{bmatrix} i_{s\alpha} \\ i_{s\beta} \end{bmatrix} + \frac{1}{\sigma} \begin{bmatrix} V_{s\alpha} \\ V_{s\beta} \end{bmatrix}$$
$$\begin{bmatrix} \frac{d\lambda_{r\alpha}}{dt} \\ \frac{d\lambda_{r\beta}}{dt} \end{bmatrix} = - \left(\begin{bmatrix} \alpha & \omega_m \\ -\omega_m & \alpha \end{bmatrix} \begin{bmatrix} \lambda_{r\alpha} \\ \lambda_{r\beta} \end{bmatrix} - \alpha L_m \begin{bmatrix} i_{s\alpha} \\ i_{s\beta} \end{bmatrix} \right) \tag{4.42}$$

Terms inside curved bracket are found exactly the same in current and flux dynamics and can be replaced by the same sliding function U. The function U is defined by the following matrix:

$$U = \begin{bmatrix} U_{s\alpha} \\ U_{s\beta} \end{bmatrix} = \begin{bmatrix} -k_{i1} sign(S_{i1}) \\ -k_{i2} sign(S_{i2}) \end{bmatrix}, \qquad where \quad \begin{matrix} S_{i1} = \widehat{i}_{s\alpha} - i_{s\alpha} \\ S_{i2} = \widehat{i}_{s\beta} - i_{s\beta} \end{matrix} \tag{4.43}$$

Hence observer expression is:

$$\begin{bmatrix} \frac{di_{s\alpha}}{dt} \\ \frac{di_{s\beta}}{dt} \end{bmatrix} = \beta \begin{bmatrix} U_{s\alpha} \\ U_{s\beta} \end{bmatrix} - \frac{R_s}{\sigma} \begin{bmatrix} i_{s\alpha} \\ i_{s\beta} \end{bmatrix} + \frac{1}{\sigma} \begin{bmatrix} V_{s\alpha} \\ V_{s\beta} \end{bmatrix}$$
$$\begin{bmatrix} \frac{d\lambda_{r\alpha}}{dt} \\ \frac{d\lambda_{r\beta}}{dt} \end{bmatrix} = - \begin{bmatrix} U_{s\alpha} \\ U_{s\beta} \end{bmatrix} \tag{4.44}$$

The gains of sliding mode terms above should be selected to steer the estimated rotor flux trajectories to the desired or actual value. here they are selected as k_{i1}=k_{i2} = $6 * 10^3$.

4.5.2 Combined SM-MRAS Speed Estimator

Now having SMO as a reference model, MRAS observer can be modeled using the following induction motor model equations as an adaptive model with ω_m being

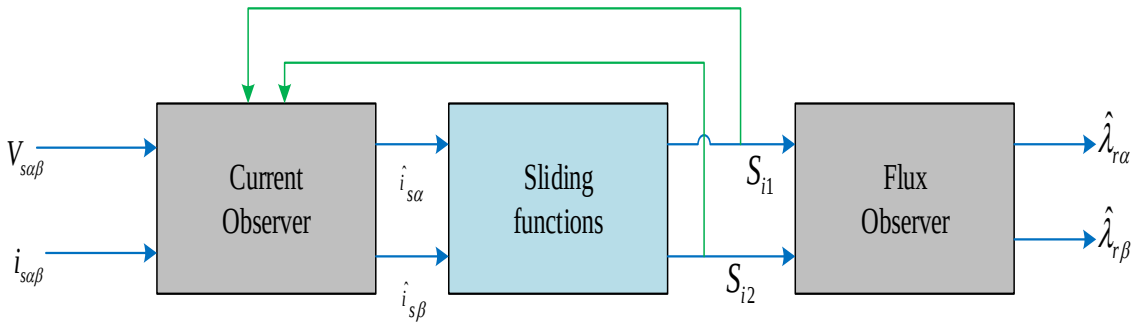

Figure 4.6: Block diagram of sliding mode rotor flux observer

adaptive quantity.

$$\begin{cases} \frac{d\lambda_{r\alpha A}}{dt} = \alpha L_m i_{s\alpha} - \alpha\lambda_{r\alpha A} - \omega_m \lambda_{r\beta A} \\ \frac{d\lambda_{r\beta A}}{dt} = \alpha L_m i_{s\beta} + \omega_m \lambda_{r\alpha A} - \alpha\lambda_{r\beta A} \end{cases} \tag{4.45}$$

The notation A in the subscripts is to mean adaptive

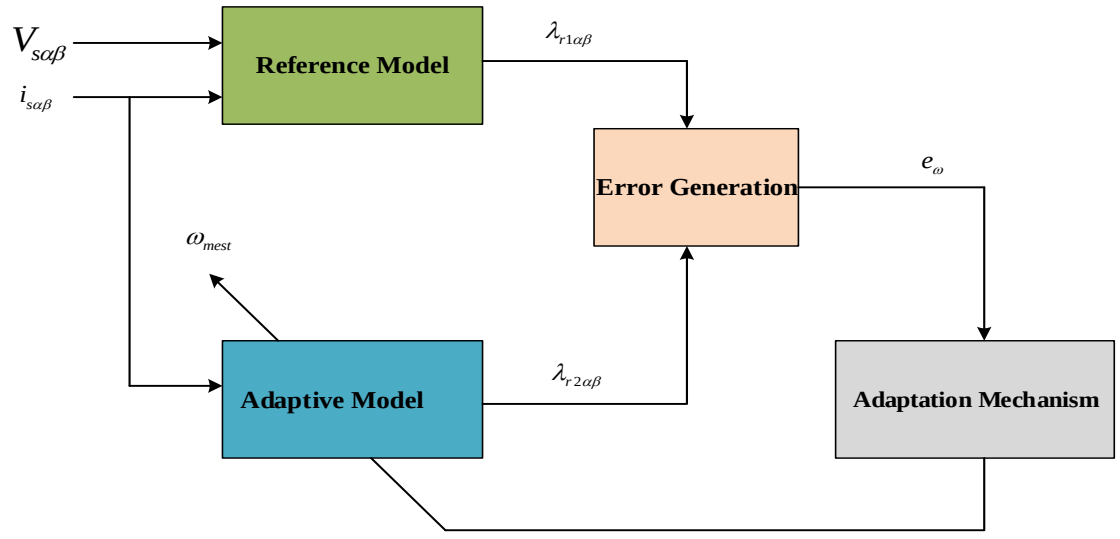

Figure 4.7: Structure of proposed Sliding mode MRAS estimator

4.5.2.1 Adaptation Mechanism

The adaptation mechanism can now be formulated using the following approach. Observers from current model (adaptive) and voltage model (reference model) can be combined and the error signal can be generated. The accuracy of MRAS estimator is highly dependent on the type of adaptation mechanism used. In this thesis sliding mode adaptation mechanism is applied in place of PI regulators used in [36] which can enhance robustness of the system since it have better tracking performance. Defining speed tuning error signal as [30]:

$$e_\omega = \lambda_{r\beta S}\lambda_{r\alpha A} - \lambda_{r\alpha S}\lambda_{r\beta A} \tag{4.46}$$

The speed-estimation adaptation law for SM scheme is derived based on Lyapunov theory to ensure stability and fast error dynamics. Defining the speed tuning signal in equation 4.46 and choosing a sliding surface as is explained in [21]:

$$S_{e\omega} = e_\omega + \lambda \int_0^t e_\omega dt \qquad for \quad \lambda > 0 \tag{4.47}$$

When the system reaches sliding surface, it gives:

$$\dot{s}_{e\omega} = \dot{e}_\omega + \lambda e_\omega = 0 \tag{4.48}$$

$$e_\omega^{'} = \lambda_{r\beta S}^{'}\lambda_{r\alpha A} + \lambda_{r\alpha A}^{'}\lambda_{r\beta S} - \lambda_{r\alpha S}^{'}\lambda_{r\beta A} - \lambda_{r\beta A}^{'}\lambda_{r\alpha S} \tag{4.49}$$

$$\begin{aligned} e_\omega^{'} = {} & \lambda_{r\beta S}^{'}\lambda_{r\alpha A} + \lambda_{r\beta S}(\alpha L_m i_{s\alpha} - \alpha\lambda_{r\alpha A} - \omega_m\lambda_{r\beta A}) \ - \lambda_{r\alpha SM}^{'}\lambda_{r\beta A} \\ & -\lambda_{r\alpha SM}(\alpha L_m i_{s\beta} + \omega_m\lambda_{r\alpha A} - \alpha\lambda_{r\beta A}) \end{aligned} \tag{4.50}$$

$$e_\omega^{'} = \underbrace{\begin{pmatrix} \lambda_{r\beta SM}^{'}\lambda_{r\alpha A} - \lambda_{r\alpha S}^{'}\lambda_{r\beta A} + \alpha L_m(i_{s\alpha}\lambda_{r\beta S} \\ -i_{s\beta}\lambda_{r\alpha S}) \ + \alpha(\lambda_{r\beta A}\lambda_{r\alpha S} - \lambda_{r\alpha AD}\lambda_{r\beta S}) \end{pmatrix}}_{f_1} - \underbrace{(\lambda_{r\alpha A}\lambda_{r\alpha S} + \lambda_{r\beta A}\lambda_{r\beta S})\hat{\omega}_m}_{f_2} \tag{4.51}$$

$$e_{\omega}^{'} = f_1 - f_2\hat{\omega}_m \tag{4.52}$$

From Lyapunov candidate function

$$V = \frac{1}{2}S^2$$

$V^{'} = SS^{'}$ Should be negative definite for stability

$$S_{e\omega}S_{e\omega}^{'} = S_{e\omega}(f_1 - f_2\hat{\omega}_m + \lambda e_{\omega}) < 0 \tag{4.53}$$

This can be attained if

$$f_1 - f_2\hat{\omega}_m + \lambda e_{\omega} \begin{cases} < 0 \quad for \quad S_{e\omega} > 0 \\ = 0 \quad for \quad S_{e\omega} = 0 \\ > 0 \quad for \quad S_{e\omega} < 0 \end{cases} \tag{4.54}$$

This can intern be achieved by using the following algorithms

$$\hat{\omega}_m = u_{eq} + u_{s\omega} \tag{4.55}$$

$$u_{eq} = \frac{f_1 + \lambda e_{\omega}}{f_2} \quad and \; u_{s\omega} = k_1 sign(S_{e\omega}) \tag{4.56}$$

The presence of f_2 in the denominator of may cause problems around zero. This problem can be overcome by magnetizing of the machine before starting up or by adding small value to it as is applied in this thesis.

Substituting equation 4.46 and 4.52 to equation 4.48 and doing some simplification the following can be obtained:

$$\begin{aligned} \dot{V} = S_{e\omega}\,\dot{S_{e\omega}} &= S_{e\omega}\left(f_1 - f_2\left(\tfrac{f_1+\lambda e_{\omega}}{f_2} + k_1 sign\,(S_{e\omega}) + \lambda e_{\omega}\right)\right) \\ &= -k_1 f_2\,(S_{e\omega} sign\,(S_{e\omega})) \end{aligned} \tag{4.57}$$

As long as k_1 is positive in the expression 4.57 is negative, which is the requirement

for Lyapunove candidate function negative definite, and stability to be guaranteed. It is the hitting control gain which can make derivative of the candidate Lyapunov function negative definite and it should be large enough to overcome the effect of external disturbances. Here the gains are $k_1 = 4 * 10^4$ and $\lambda = 0.5$.

4.6 Chattering Minimization in SMC

Although to account for the presence of modeling imprecision and of disturbances the control law has to be discontinuous across the sliding surface $s(t)$, switching is not instantaneous and value of $s(t)$ is not known with infinite precision. This leads to oscillations in the state vector at finite frequency, referred to as chattering. It results in high heat losses in electrical power circuits, high wear of moving mechanical parts such as actuators and low control accuracy. Therefore, sliding mode controllers given so far will have chattering near sliding surface due to the presence of signum function. For the controller to perform properly this chattering phenomenon must be eliminated. This can be achieved by smoothing out the control discontinuity in a thin boundary layer neighboring the switching surface. This approximation can be implemented by using the quasi-sliding mode, using saturation or sigmoid function in place of signum function [13, 16, 30].

$$sign(s) = \begin{cases} -1 \quad if \quad s < 0 \\ 0 \quad if \quad s = 0 \\ 1 \quad if \quad s > 0 \end{cases}, \quad sat(s) = \begin{cases} -1 \quad if \quad s < -\varepsilon \\ \frac{s}{\varepsilon} \quad if \quad |s| = \varepsilon \\ 1 \quad if \quad s > \varepsilon \end{cases}, \quad sigm(s) = \left(\frac{2}{1 + e^{-\gamma s}}\right) - 1$$

Where, ε is a small positive number defining the boundary layer of saturation function and γ is also a small positive number adjusting the slope of sigmoid function.

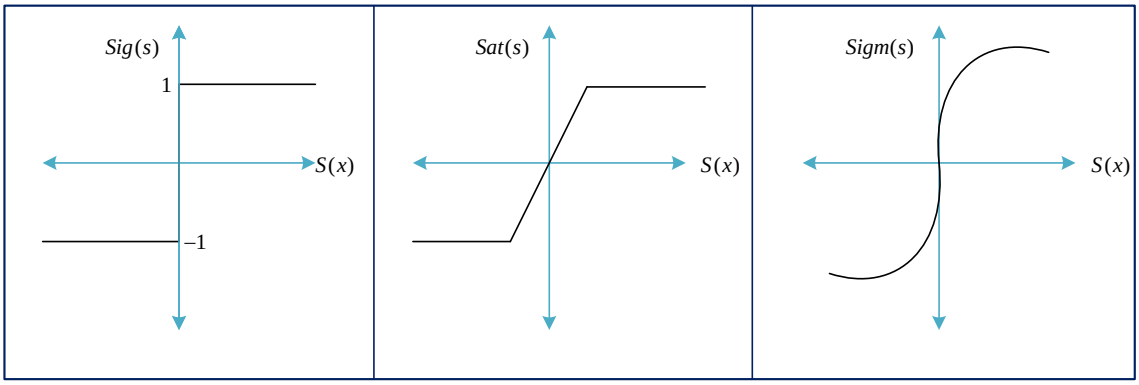

Figure 4.8: Signum, Saturation and Sigmoid functions

This work does minimization of chattering by using sigmoid approximation and the effect is discussed by using clear simulation waveforms in section 5.3.1.

Chapter 5

Simulation Result and Discussion

5.1 Introduction

Computer modeling and simulation is the usual way of studying the behavior of proposed real-life systems and to decide whether new control algorithms are valid in order to avoid mistakes early in simulations before actual hardware implementation. Among various simulation software packages, SIMULINK is one of the most common and powerful technique for simulating dynamical systems due to its graphical interface and simplicity. SIMULINK uses MATLAB as a tool for mathematical purposes which further enhance modeling process. In the following sections, analysis of different analytical considerations of the proposed control scheme in previous sections are verified by simulations.

5.2 Simulink Model of Feedback Linearized Induction Motor Control Using FOSMC and Sliding Mode-MRAS Estimator

A complete SIMULINK diagram of proposed system is shown in figure 5.1 below. The induction motor used is the squirrel cage induction motor with the parameters

presented in table A.1. Here PID, SMC FOSMC speed controller with SVPWM and SM-MRAS estimator is simulated. Those controllers are tested for speed and rotor flux tracking performance and for robustness to load torque disturbance under different operating conditions and then from the results obtained comparison of controller is performed. The induction motor stator is powered by SVPWM controlled VSI and speed is controlled by fractional order sliding mode controller with input output feedback linearization which enables independent control of rotor flux and torque. The output of IOFL are SVPWM reference signals used generate gate signals of inverter switches to supply the induction motor so that it can run with the required speed command.

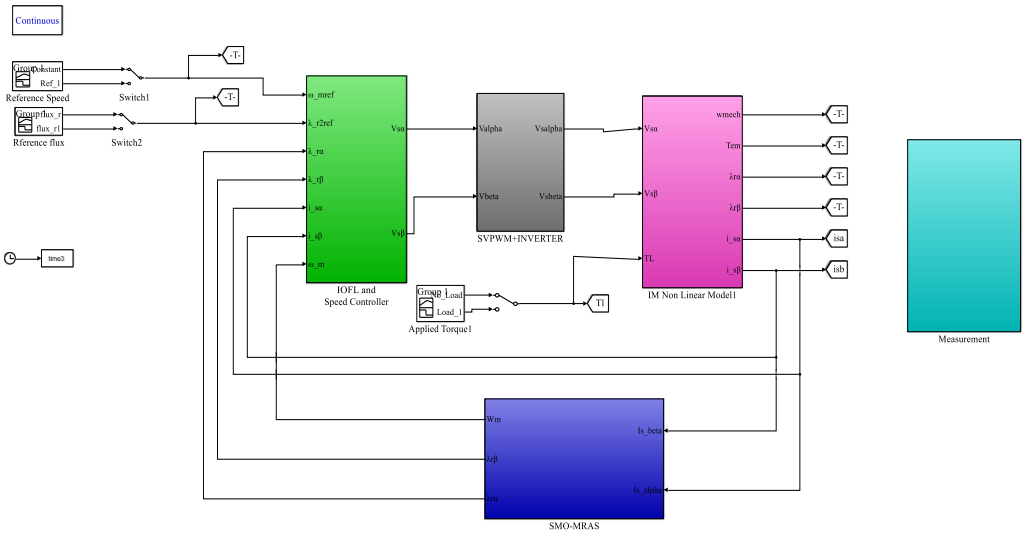

Figure 5.1: Simulink Model of IOFL and Speed Controller

5.3 Simulation Results

To test the behavior of squirrel cage induction machine with nonlinear control, three simulation tests are performed. In the first test, behavior of the machine during unloaded start, then introducing a load torque of 10 Nm with indicated profiles is studied with simulations.

5.3.1 Chattering Effect of sliding mode controller in the speed loop

Chattering is undesirable oscillations resulting from ideal infinite frequency control signal.

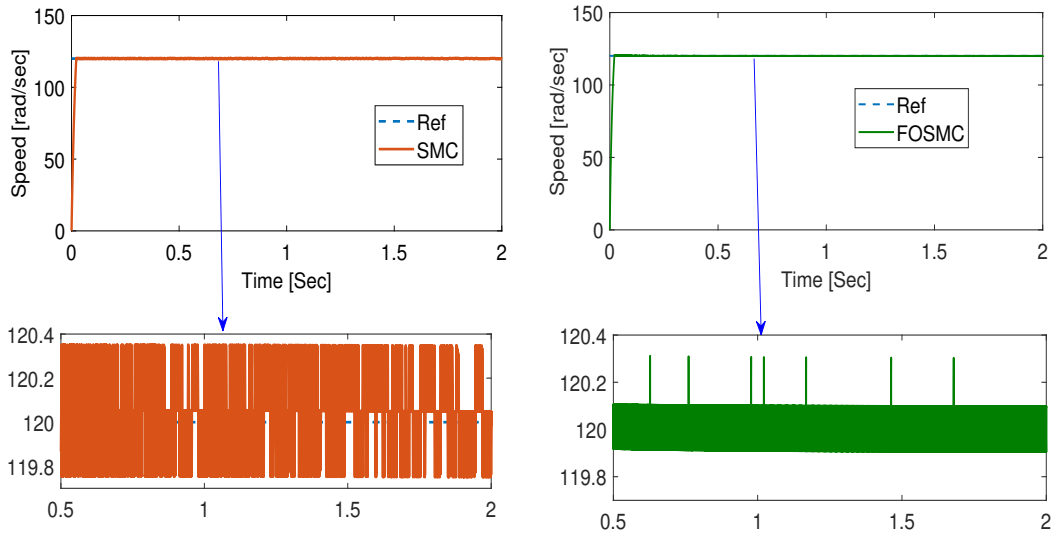

Figure 5.2: Speed Response Using Signum

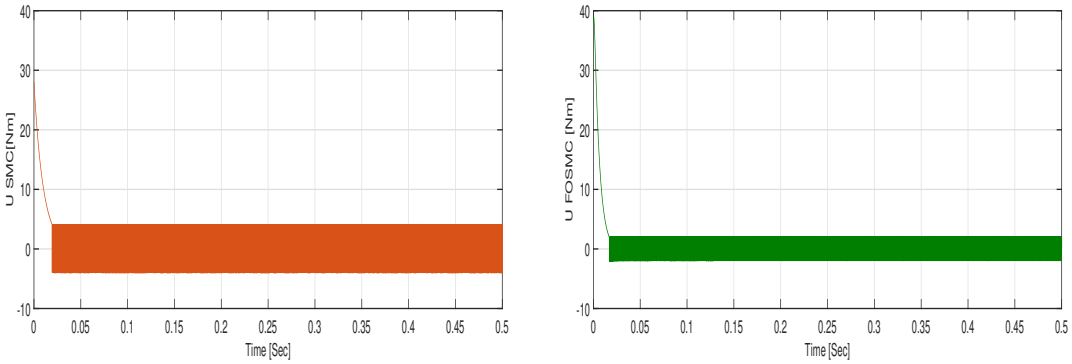

(a) (b)

Figure 5.3: Control inputs for SMC and FOSMC

Waveforms in Figure 5.2 (left top) are obtained using $sign(S_\omega)$ function and waveforms for SMC and Figure 5.2 (right top) obtained by using $sign(S_\omega)$ function for

FOSMC. From the plots we can easily observe that application of $sign(S_\omega)$ leads excessive oscillation in the output and chattering effect in the control input which is undesirable for induction motor drive system. Figure 5.3 illustrates the control output (T_{em}) obtained from SMC in Figure 5.3a and FOSMC in Figure 5.3b by using $sign(S_\omega)$ for the speed control loop. From the plots it can be shown that FOSMC have minimized chattering amplitude than that of integer order SMC. Even though chattering is reduced by utilizing FOSMC it still presents. By approximating the *sign* function this chattering effect can be avoided. Simulation plots in the coming sections are obtained by utilizing continuous sigmoid function instead of *sign* function.

5.3.2 Response of Controllers for Noise

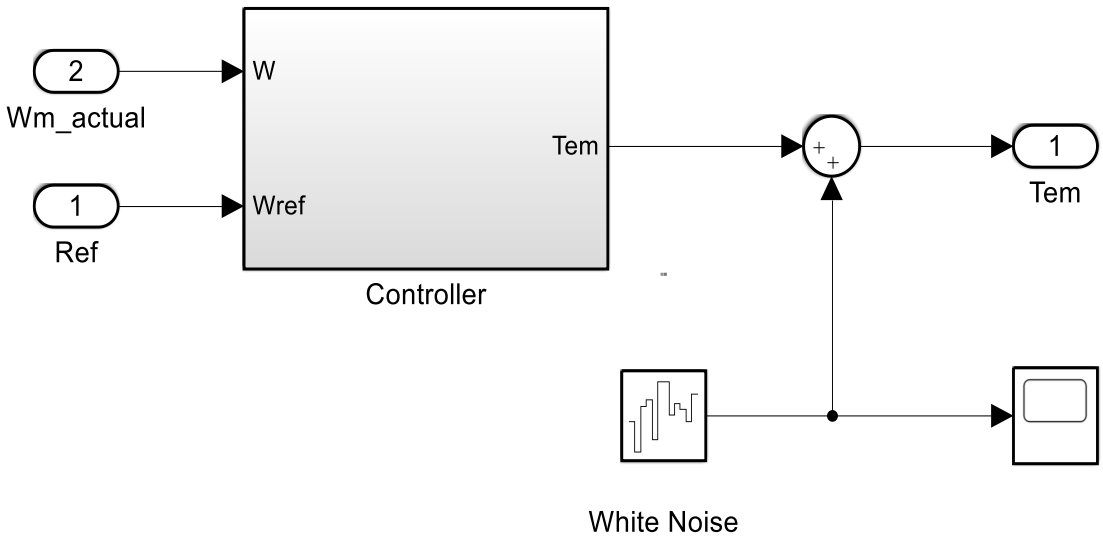

Figure 5.4: Noise on the controller side

Figure 5.4 shows the applied noise added up with the controller output or electromagnetic torque reference. The effect of this noise is observed for PID, SMC, and FOSMC.

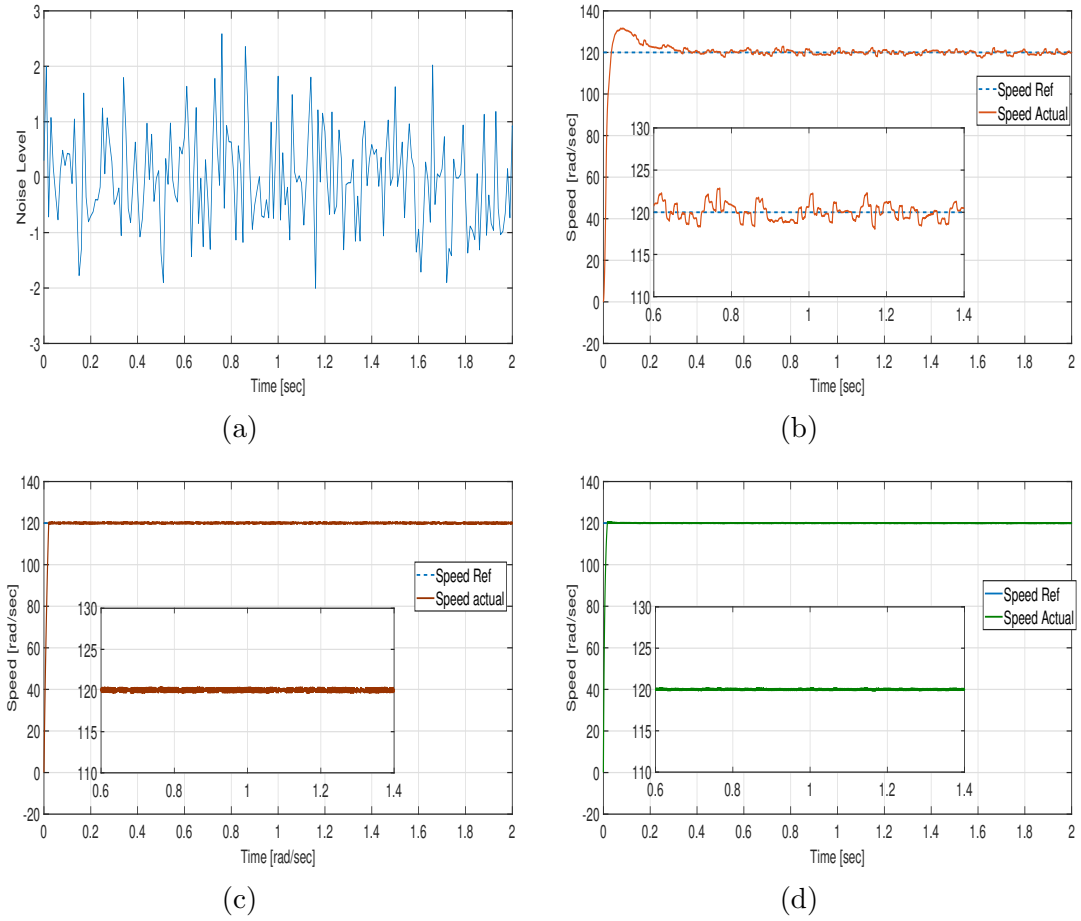

Figure 5.5: Response of speed controllers for noise

Responses of controllers for PID, SMC, and FOSMC for the indicated noise of Figure 5.5a in the controller are given in plots Figure 5.5b, Figure 5.5c and Figure 5.5d respectively. From these response plots it can be observed that PID controller having worse irregularities or sever oscillations in the output while SMC and FOSMC shows more robustness for such a noise.

5.3.3 Operation at a constant speed

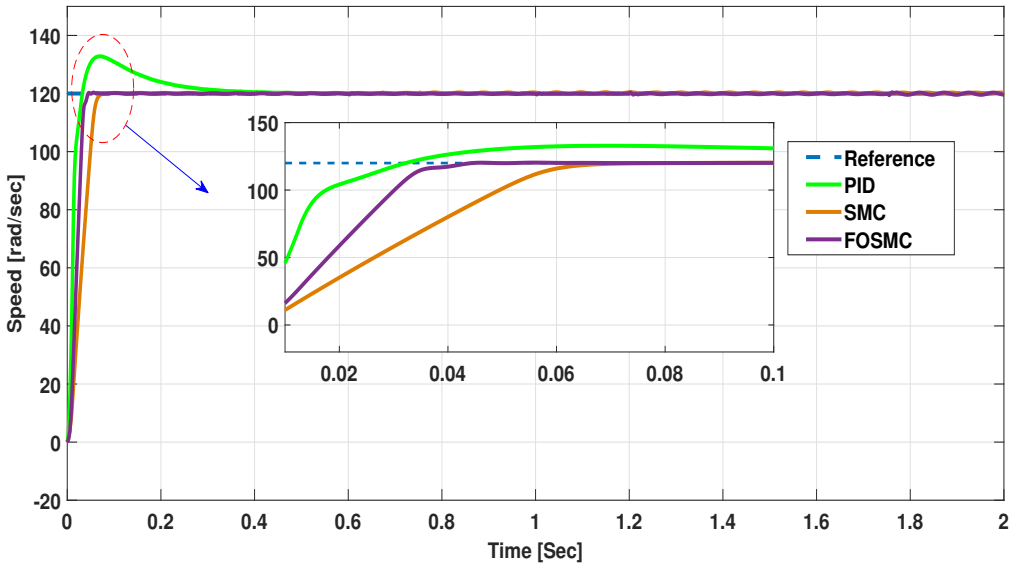

Figure 5.6: Speed responses for a constant speed at Normal condition

Figure 5.6 presents responses of PID, SMC and proposed FOSMC. Here the reference speed is set at 120 rad/sec and rotor flux magnitude is kept at 3 Wb. Behaviors of each controller are noticed at no load condition simulating it for 3 seconds in response to these reference commands. As it can be inferred from the plots all controllers track the reference command signal at steady state. But, the way that they reach this steady state value is different. Even though, PID controller have less steady state error it shows sever overshoot of 9.5211% at starting up while SMC and FOSMC waveforms shows overshoots of 0.4753% and 0.3674% respectively. Even though PID controller have faster rise time of 0.0209 seconds, it settles to the final desired value slowly with settling time of 0.2417 seconds. FOSMC rises and settles faster, with a rise time of 0.0235 second and settling time of 0.0405 seconds, than integer order SMC having a rise time of 0.0434 seconds and settling time of 0.0627 seconds.

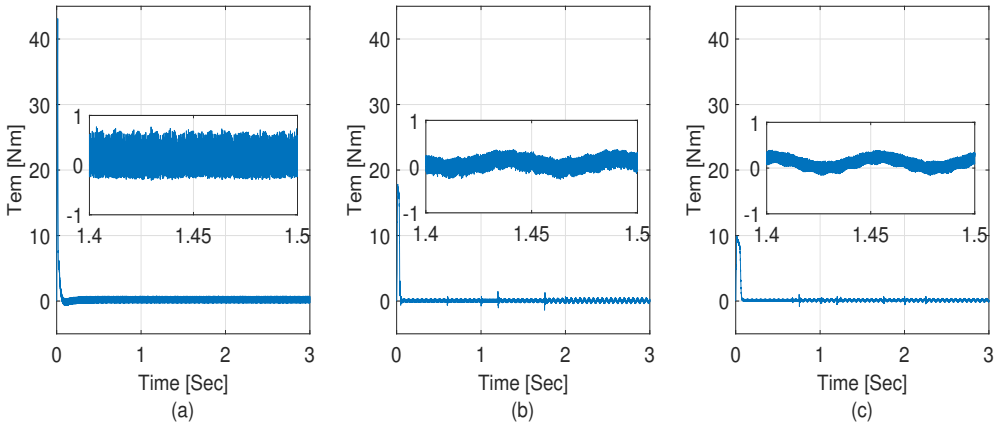

Figure 5.7: Torque Responses under no load condition

Figure 5.7 presents the simulated result for developed electromagnetic torque. Simulation has been carried out again for 3 secs and obtained results of the three controllers were presented with their corresponding zoom view around zero in $(1.4 \rightarrow 1.5)$ second time range. It can be noticed that SMC and FOSMC shows better performance in terms of torque ripple minimization.

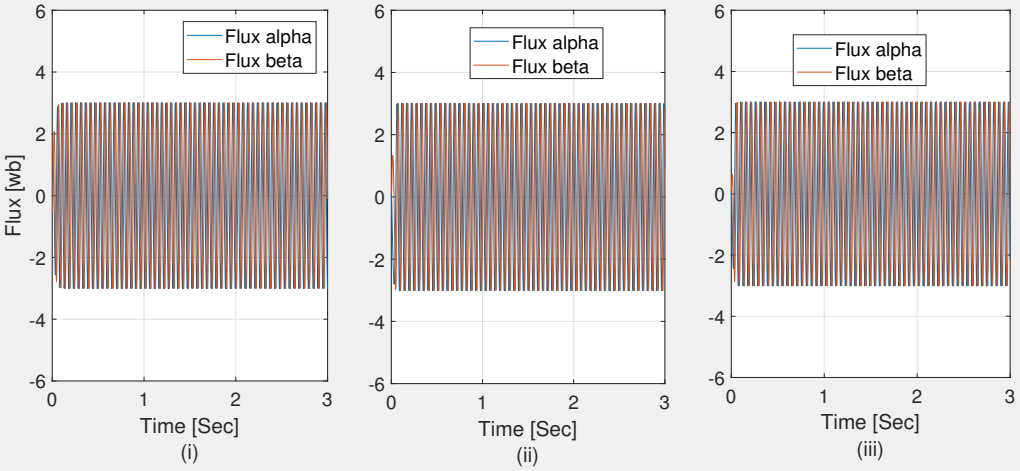

Figure 5.8: Alpha beta frame flux response

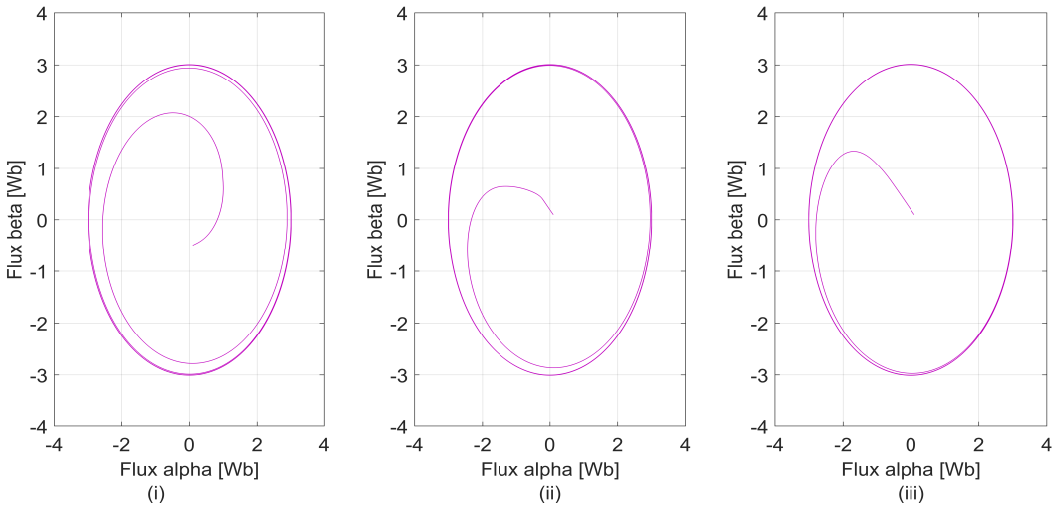

Figure 5.9: Alpha beta Flux Trajectory

Figures 5.8 presents rotor flux in (α, β) axis component and their corresponding circular trajectory were also presented in figure 5.9. These plots show no significant difference in the responses showing that good performance of IOFL used. But, FOSMC have better responses offering well defined circular trajectory than SMC and PID.

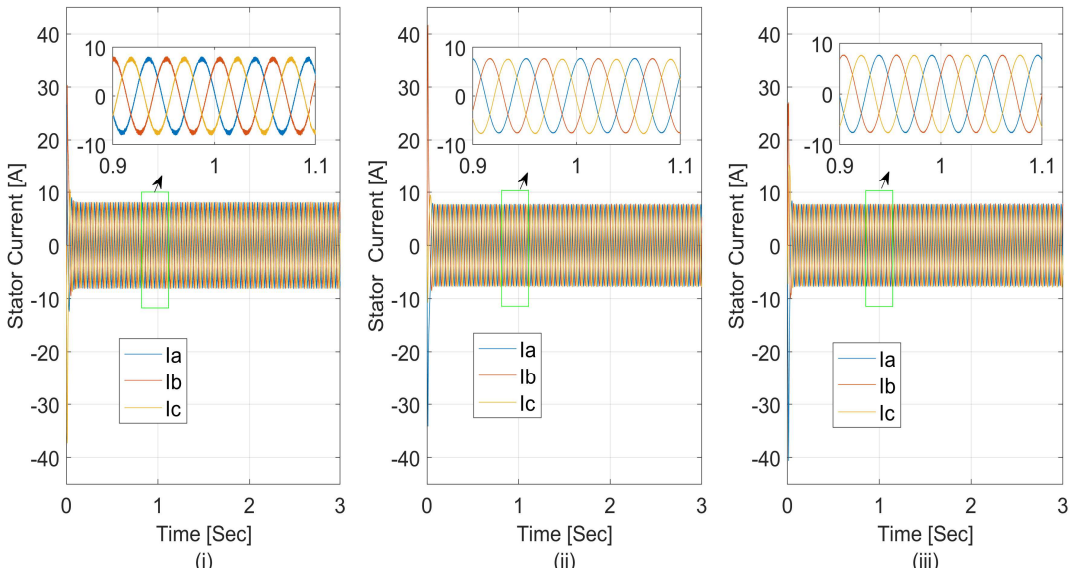

Figure 5.10: Stator currents at no load

5.3.4 Operation at varying speed reference

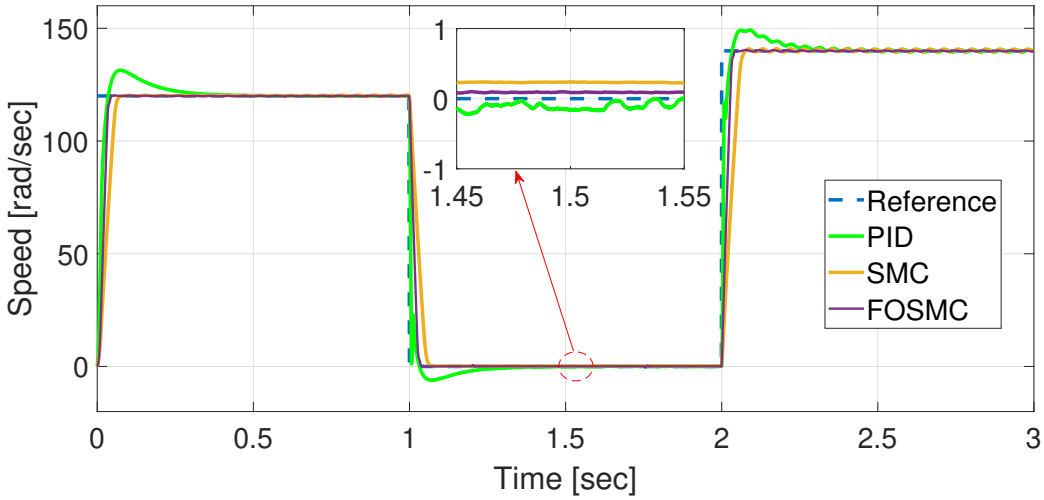

Figure 5.11: Response for a varying speed command at no load

Figure 5.11 above presents speed response for a command profile set at $120\,rad/s\,e\,c$ for $(0 \rightarrow 1)$ seconds, $0\,rad/s\,ec$ seconds for $(1 \rightarrow 2)$ seconds and $140\,rad/s\,ec$ for $(2 \rightarrow 3)$ seconds. Response plots clearly show that both SMC and FOSMC results better responses than PID controllers as it is characterized by higher overshoots during starting and at instants when speed change takes place. FOSMC follows this changing reference command faster than its equivalent integer order SMC. Another important quality of these controllers that can be examined from the zoomed view presented above for $(1.45 \rightarrow 1.55)$ seconds is zero speed operation. In this operation time FOSMC shows superior performance by having minimum steady state error. It can be inferred that FOSMC shows better dynamical responses even at low speed operations or particularly zero speed operation.

5.3.5 Operation at varying flux reference

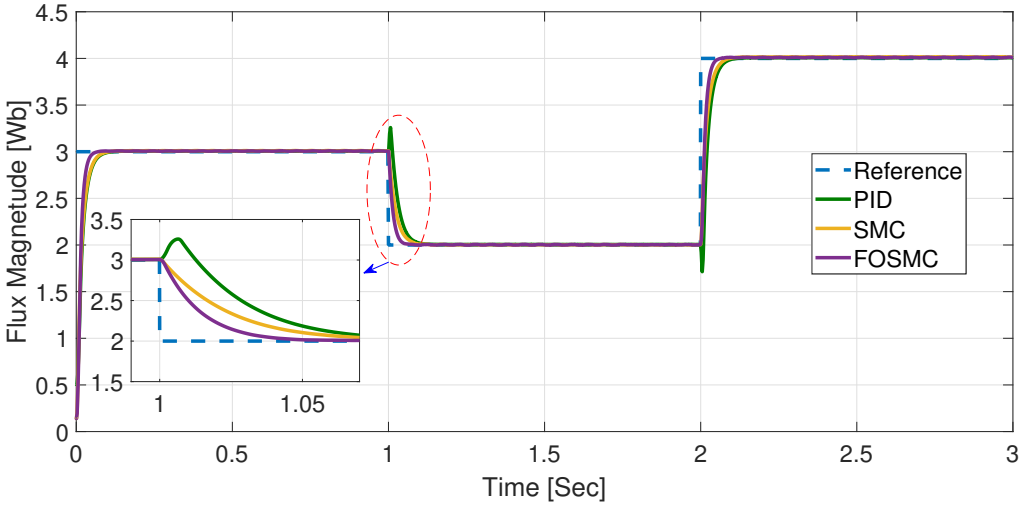

Figure 5.12: Response for varying flux reference

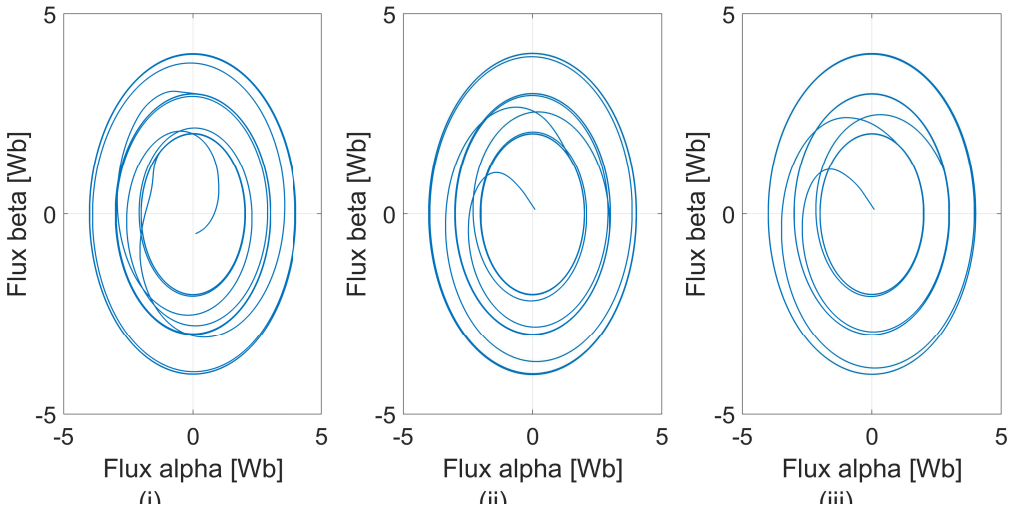

Figure 5.13: Flux trajectory for three controllers

Figure 5.13 presents frame rotor flux trajectory for the varying reference flux magnitude presented in figure 5.12. As it can be noticed from those plots best tracking of varying flux is obtained using this controller. Here it is justified how to control the rotor flux using the actual nonlinear model with no need of orientation concept to linearize the nonlinear behavior of squirrel cage induction motor.

5.3.6 Operation at load disturbed condition

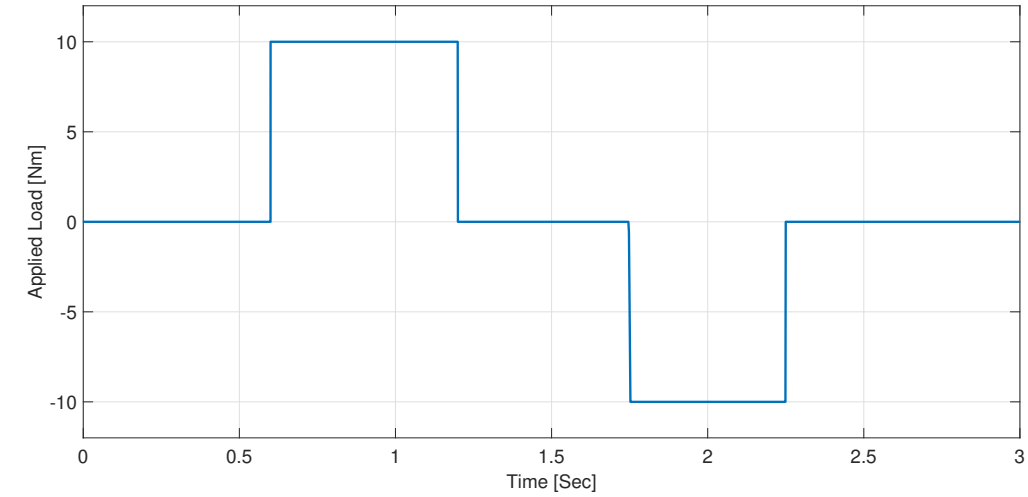

(a)

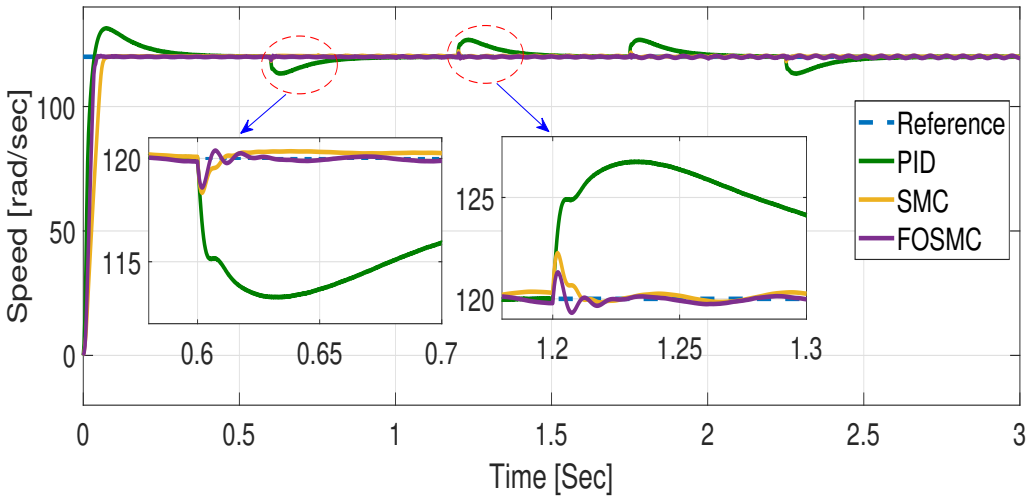

(b)

Figure 5.14: Speed tracking performance (b) for applied load of (a)

Simulation results in figure 5.14b show that speed droppings and over speeds are sever in PID controllers due to the introduction of load disturbance of profile presented in figure 5.14a. Zoomed views in this plot also reveals that SMC's result higher deviations than FOSMC during the introduction of FOSMC. To clearly compare robustness of those controllers for load torque disturbance, speed drops at the instant when a load torque is applied at 0.75 second can be quantified as 5.5982% using PID

speed controllers, 1.388% when SMC is used and 1.1757% when FOSMC is applied.

5.4 Simulation of sliding mode MRAS Estimator

To highlight the performance and robustness of the proposed algorithm for rotor flux and rotor speed estimation, a variety of cases have been simulated and will be presented later. The static and dynamic performance of the rotor flux observer are analyzed from the simulation of the following modes of operation:

- No-load operation
- Variation of the load torque and
- Low speed operation

No-load Operation

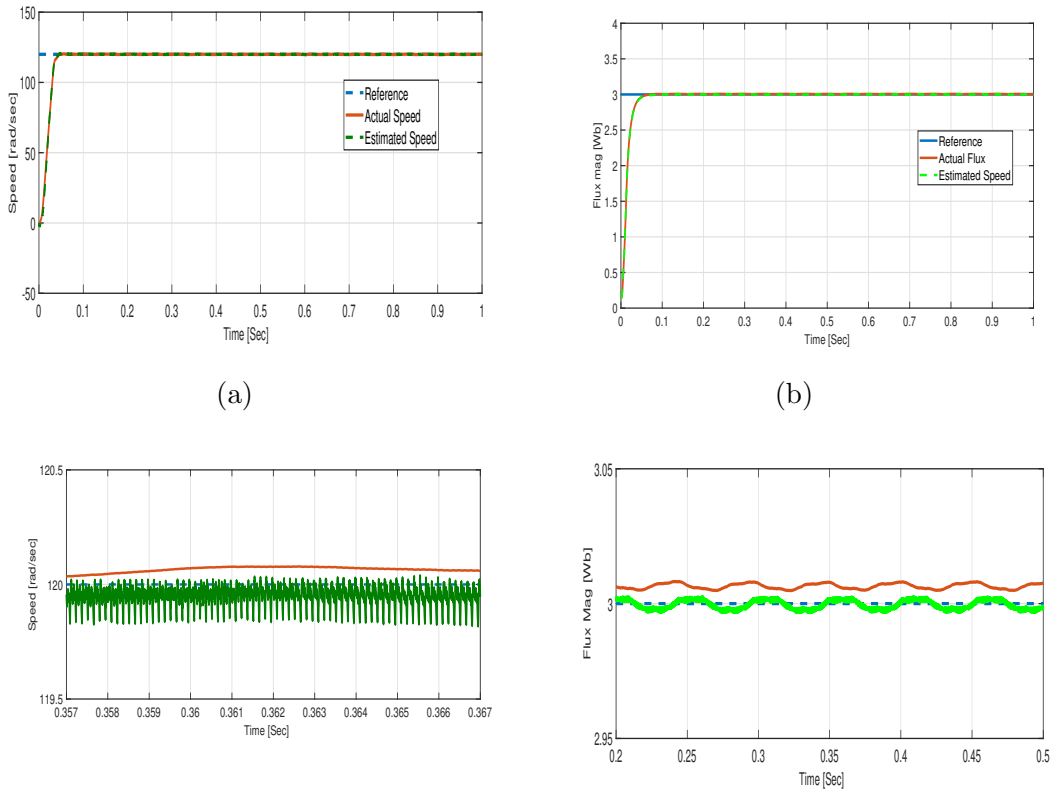

Figure 5.15: Speed and flux estimation performance at unloaded condition

Figure 5.15 illustrates the response of the actual speed in 5.15a with their zoom in 5.15c and the estimated rotor flux magnitude in 5.15b and their zoom in 5.15d using IOFL and FOSMC for closed loop speed compensation. Figure 5.16 below shows estimation error of speed and flux in 5.16a and 5.16b respectively. It can be seen that the estimator gives a minimized speed and flux estimation error. Mean absolute percentage error is 0.1767% for speed estimation and 0.2584% for rotor flux estimation. As can be seen in Figure, it is important to note that the system demonstrates good estimation capability under fairly good operating conditions.

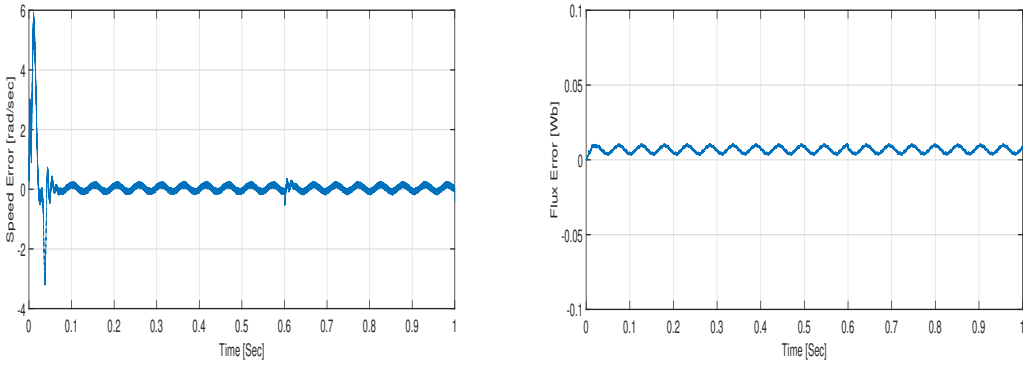

(a) (b)

Figure 5.16: Speed estimation error (a) and Flux estimation error (b)

5.4.1 Estimation performance for a varying speed and Load

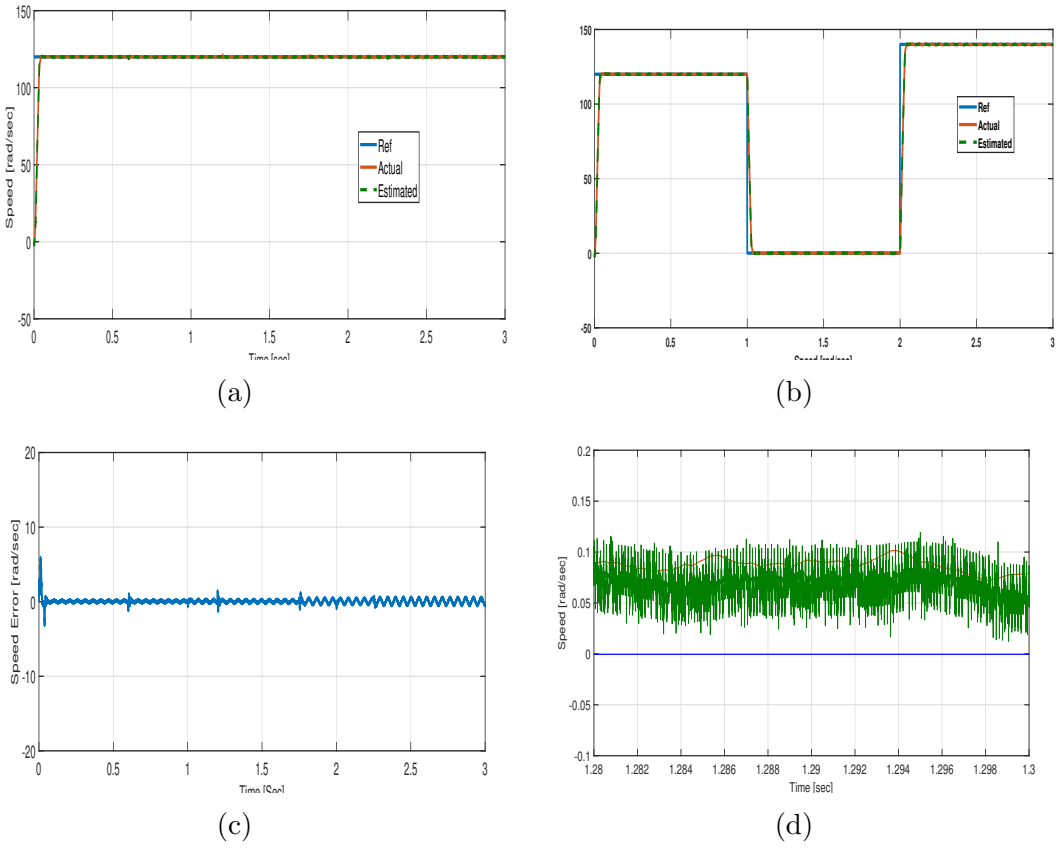

Figure 5.17: Estimation for a varying speed and load

Observing Figure 5.17 speed estimation performance for loaded case with constant reference in 5.17a and varying reference in 5.17b. Estimated speed almost follows actual speed trajectory even during the introduction of load torque and varying commands set with a mean absolute percentage estimation error of 0.1772%. From the varying speed reference responses presented before, estimation performance under low speed operation particularly zero speed operation can be noticed. Here estimated speed tracks the actual speed even in zero speed range of operation as can be inferred from the zoomed views around zero.

Chapter 6

Conclusion and Future Work

6.1 Conclusion

In this thesis work sensor less control of squirrel cage induction motor from its nonlinear model is developed it is used in the entire development considerations of this thesis. Closer look of the model shows the squirrel cage induction motor is a nonlinear multi-variable, strongly coupled system.

The second part of this work then focuses on the modeling of proposed controller and observer. Input output feedback linearization technique which is proved by many literature for providing improved responses for nonlinear systems is applied for squirrel cage induction motor system and promising decoupled control of rotor flux and torque is obtained. Torque and flux are independently controlled using IOFL and different speed controller are used to generate electromagnetic torque reference. Aiming that to improve the performance of the machine, namely tracking of reference trajectories and disturbance rejection three controllers namely PID, SMC, and FOSMC are applied for the speed loop. Generally, the application of fractional order sliding mode controller with input output feedback linearization results better performance considering the following:

- Minimized overshoot, faster settling to the required command, less torque ripples, best low speed operation tracking quality. FOSMC shows superior perfor-

mance for those qualities by having least overshoot of 0.3674%, fastest settling time of 0.0405 seconds, and least speed drop of 1.1757% for the application of 10 Nm.

- Performance comparison from simulation results reveal that under load torque disturbance IOFL with FOSMC shows less speed drop. Hence it can be concluded that IOFL-FOSMC have best robustness quality.

It is observed that input output feedback linearization by its own could not guarantee for high performance application of the drive as it requires all the states to be accessed by measurements. To tackle this problem and benefit more from nonlinear controller this thesis developed an estimation algorithm that can extract inaccessible states (rotor fluxes) and states requiring costly installation (speed) by having only stator current information. Sliding mode model reference adaptive system estimator is found more suitable for estimation of speed for high performance applications. Its detailed formulation is studied and simulation results section show that the applied sliding mode model reference adaptive system estimator gives good estimate of rotor flux and speed with mean absolute percentage error of 0.2584% and 0.1767% respectively.

6.2 Future Work

Application of the techniques applied in this work on the induction machine for generator operation: As induction generators are commonly used sort of machines used for generation of electricity in areas like wind power and hydro power generation systems it would be very important to apply this technique for those machines too.

Efficiency Optimization: One of the strengths of this thesis work is getting interesting rotor flux trajectory tracking performance. Hence optimal rotor flux reference can be generated for optimization of motor efficiency. Future improvement of this work can be made with the application of intelligent optimization techniques for

efficiency maximization of this motor.

Practical realization with FPGA: Nowadays, FPGAs are becoming popular processors having fast processing speed and computational efficiency. Hence the algorithms developed in this thesis could be realized with those processor families for its betterment.

Bibliography

[1] K. N. Gyftakis, D. V. Spyropoulos, J. C. Kappatou, and E. D. Mitronikas, "A novel approach for broken bar fault diagnosis in induction motors through torque monitoring," *IEEE Transactions on Energy Conversion*, vol. 28, no. 2, pp. 267–277, June 2013.

[2] A. Hashim, O. Ahmed, and M. W. Dunnigan, "Combined Sliding Mode Control With a Feedback Linearization for Speed Control of Induction Motor," *2010 1st International Conference on Energy, Power and Control (EPC-IQ)*, vol. 7, no. 1, pp. 19–24, 2011.

[3] M. V. Riccardo, Patrizio Tomei Cristiano, *Advances in industrial control*. Springer US, 2009.

[4] P. Vas, *Sensorless Vector and Direct Torque Control*. NEW YORK: OXFORD UNIVERSITY PRESS, 1998.

[5] V. H. Duy, I. Zelinka, and H.-s. Choi, *AETA 2015: Engineering and in Electrical Recent Advances Related Related Sciences*. Vietnam: Springer US, 2015.

[6] J. G. Haitham Abu-Rub, Atif Iqbal, *HIGH PERFORMANCE CONTROL OF AC DRIVES WITH MATLAB / SIMULINK MODELS HIGH PERFORMANCE CONTROL OF AC DRIVES WITH MATLAB / SIMULINK*. Chichester, West Sussex: A John Wiley & Sons, Ltd., Publication, 2012.

[7] N. Mohan, *Advanced Electric Drives*. New Jersey: John Wiley & Sons, Inc, 2014.

[8] T. F. C. K. Shi, *APPLIED INTELLIGENT CONTROL OF INDUCTION MOTOR*, 1st ed. John Wiley & Sons (Asia) Pte Ltd: John Wiley & Sons (Asia) Pte Ltd, 2011.

[9] A. Ammar, A. Bourek, and A. Benakcha, "Nonlinear SVM-DTC for induction motor drive using input-output feedback linearization and high order sliding mode control," *ISA Transactions*, 2017.

[10] W. Tatek and M. Mamo, "Model Reference Adaptive Control Based Sensorless Speed Control of Induction Motor," *International Journal of Scientific & Engineering Research Volume*, vol. 8, no. 6, pp. 2175–2276, 2017.

[11] B. Kumar, C. Ygesh K, and S. P. Singh, "MRAS based Speed Estimation Strategies for Induction Motor Drives: A review," *IEEE*, pp. 7–10, 2016.

[12] P. Roy, S. Sarkar, B. K. Roy, and N. Singh, "A Comparative Study between Fractional Order SMC and SMC Applied to Magnetic Levitation System," in *2017 Indian Control Conference*. Guwahati: IEEE, 2017, pp. 473–478.

[13] X. Wang, *Advanced Sliding Mode Control for Mechanical Systems*. Beijing: Springer US, 2012.

[14] S. Ebrahimkhani, "Robust fractional order sliding mode control of doubly-fed induction generator (DFIG)-based wind turbines," *ISA Transactions*, 2016.

[15] J. Huang, H. Li, Y. Chen, and Q. Xu, "Robust Position Control of PMSM Using Fractional-Order Sliding Mode Controller," *Abstract and Applied Analysis*, 2012.

[16] N. Bouarroudj, D. Boukhetala, and F. Boudjema, "Sliding-Mode Controller Based on Fractional Order Calculus for a Class of Nonlinear Systems," *International Journal of Electrical and Computer Engineering (IJECE)*, vol. 6, no. 5, p. 2239, 2017.

[17] A. M. Concepción, C. YangQuan, and B. M. Vinagre, "Chapter 1," in *Fractional-order Systems and Controls. Advances in Industrial Control.* London: Springer, 2010, ch. One, pp. 3–8.

[18] Chengbin Ma, "Fractional Order Control and Its Applications in Motion Control," Ph.D. dissertation, The University of Tokyo, 2014.

[19] A. Tepljakov, E. Petlenkov, and J. Belikov, "FOMCON : Fractional-Order Modeling and Control Toolbox for MATLAB," in *Proceedings of the 18th International Conference Mixed Design of Integrated Circuits and Systems-MIXDES 2011.* IEEE, 2011, pp. 684–689.

[20] Y. Chen and I. Petr, "Fractional Order Control - A Tutorial," in *2009 American control conference.* St. Louis, MO, USA: IEEE, 2009, pp. 1397–1411.

[21] S. M. Gadoue, D. Giaouris, and J. W. Finch, "Performance evaluation of a sensorless induction motor drive at very low and zero speed using a MRAS speed observer," *IEEE Region 10 Colloquium and 3rd International Conference on Industrial and Information Systems, ICIIS 2008*, pp. 8–13, 2014.

[22] Meziane.Salima, Toufouti.Riad, and Benalla. Hocine, "APPLIED INPUT-OUTPUT LINEARIZING CONTROL FOR HIGH-PERFORMANCE INDUCTION MOTOR," *Journal of Theoretical and Applied Information Technology*, pp. 7–15, 2014.

[23] M. Zaky, M. Khater, H. Yasin, S. Shokralla, and A. El-Sabbe, "Speed-sensorless control of induction motor drives (review paper)," *Engineering Research Journal (ERJ), Faculty of Engineering, Minoufiya University, Egypt, ISSN 1110-1180*, vol. 30, pp. 433–445, 10 2015.

[24] S. Xepapas, A. Kaletsanos, F. Xepapas, and S. Manias, "Sliding-mode observer for speed-sensorless induction motor drives," *IEE Proceedings - Control Theory and Applications*, 20013.

[25] P.S. Bimbhra, *[BOOK]electrical machinery,dr p s bimbhra.PDF*, 7th ed. New Delhi: KHANNA PUBLISHERS, 2009.

[26] Z. Salleh, P. Melaka, F. A. Patakor, and M. Politechnic, "STUDY ON PARAMETER DETERMINATION FOR 1 . 5KW AC INDUCTION MOTOR," in *Seminar Penyelidikan Zon Utara 2013*, no. January 2014, Syed Sirajuddin, 2013.

[27] S. Pradeepa, "Adoption of SVPWM Technique to CSI and VSI," *2018 3rd International Conference for Convergence in Technology (I2CT)*, pp. 1–6, 2018.

[28] I. Iqbal, A. Adoum, and Mohibullah, "Matlab/Simulink Model of Space Vector PWM for Three-Phase Voltage Source Inverter," in *Proceedings of the 41st International Universities Power Engineering Conference*, vol. 2, no. 2, 2006, pp. 1096–1100.

[29] H. A. Sher, *Simulation of Power Electronic Circuits using SIMULINK*, 2013.

[30] S. Zaidi, F. Naceri, and R. Abdssamed, "Input-Output Linearization of an Induction Motor Using MRAS Observer," vol. 68, pp. 49–56, 2014.

[31] H. J. Marquez, *NONLINEAR CONTROL SYSTEMS*. New Jerse: John wiley & SONS, INC., PUBLICATION, 2013, no. 4.

[32] S. . Li, *APPLIED NONLINEAR CONTROL*, 1991.

[33] M. Bill and T. Dawn, "Control Tutorials for MATLAB and Simulink - Motor Position_ Root Locus Controller Design," 2017. [Online]. Available: http://ctms.engin.umich.edu/CTMS/index.php?example=MotorPosition{&}section=ControlRootLocus

[34] F. Benchabane and A. Titaouine, "Systematic Fuzzy Sliding Mode Approach Combined With Extented Kalman Filter for Permanent Magnet Synchronous Motor control," no. 06, 2014.

[35] C. B. Regaya, F. Farhani, and A. Zaafouri, "AN ADAPTIVE SLIDING-MODE SPEED OBSERVER," vol. 11, no. 4, pp. 763–771, 2017.

[36] M. A. Husain, "MRAS based Sensorless Control of Induction Motor based on Rotor Flux," *2018 International Conference on Computational and Characterization Techniques in Engineering & Sciences (CCTES)*, pp. 152–155, 2018.

Appendix A

Appendix 1

A.1 Parameters

Table A.1: Parameters used in simulations

		Symbol	Value
Induction motor [26]	Stator Resistance	R_s	4.6 Ω
	Rotor Resistance	R_r	4.35 Ω
	Stator inductance	L_s	0.3382 H
	Rotor inductance	L_r	0.3382 H
	Mutual inductance	L_m	0.3210 H
	Pole pairs	p	2
	Coefficient of friction	f_r	0.001 $Nm.s.rad^{-1}$
	Moment of inertia	J_{eq}	0.004 Kgm^2
Estimator	Reference Model	k_{i1}	6000
		k_{i2}	6000
	Adaptation	λ	0.5
		k_1	4000
		k	5
Controller	IOFL	k_{a1}	80000
		k_{b1}, k_{b2}	40000, 80000
	SMC	λ_1	0.5
		K_r	5
		K_s	2000
	FOSMC	λ_1	0.5
		K_r	5
		K_s	2000
		α	0.2
	PID	k_p	0.924
		k_i	8.4
		k_d	0.0084

A.2 Motor Open loop model

Figure A.1 is the model of of squirrel cage induction motor constructed SIMULINK

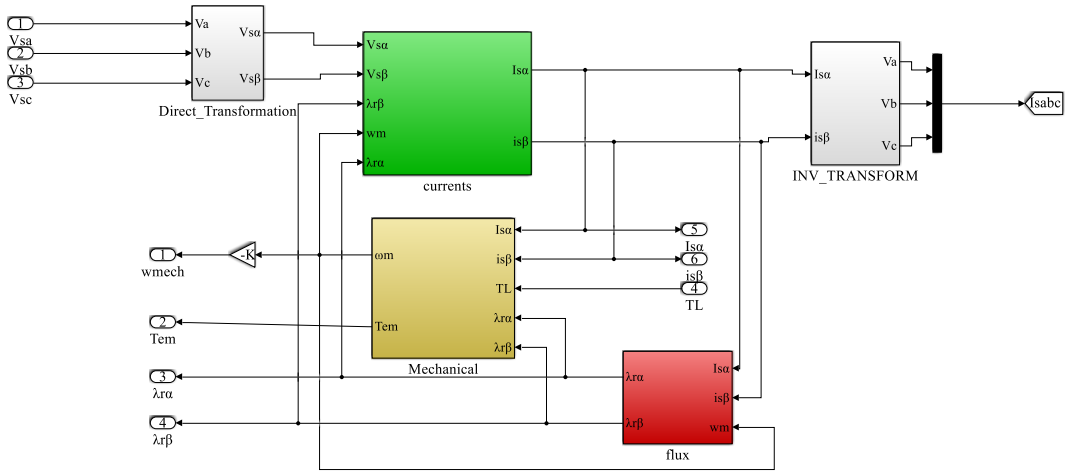

Figure A.1: Open loop Simulink model of SCIM

A.3 Inside View of IOFL block

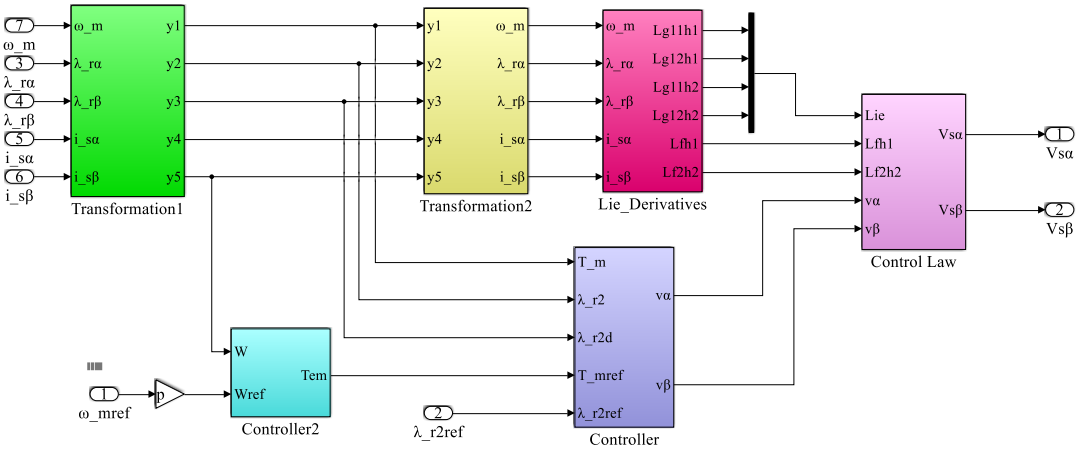

Figure A.2: Inside view of IOFL Simulink model

A.4 SMO-MRAS Estimator

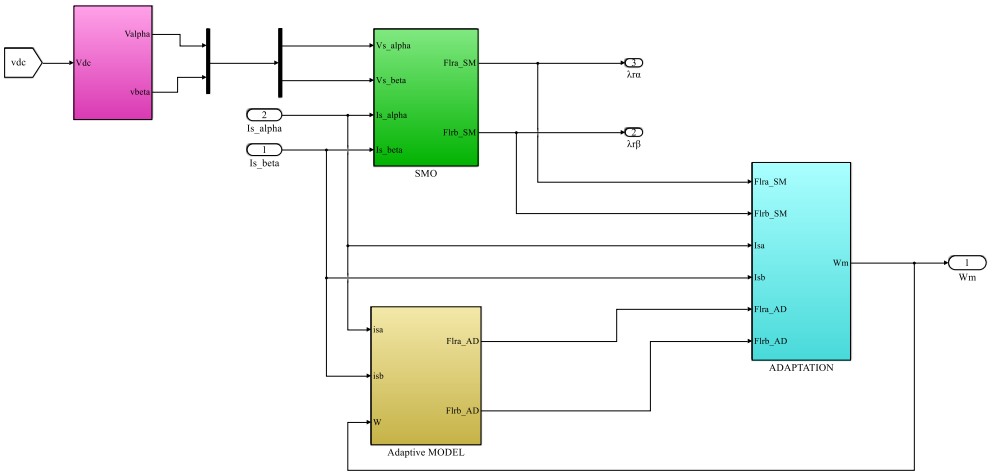

Figure A.3: Simulink block of SMO-MRAS Estimator

A.5 SVPWM code

```
%Sector===================================
function Scr = S(Valpha,Vbeta)
alpha=atan2(Vbeta,Valpha)*180/pi;
if alpha>=0&&alpha<60
    Scr=1;
elseif alpha>=60&&alpha<120
    Scr=2;
elseif alpha>=120&&alpha<180
    Scr=3;
elseif alpha>=-180&&alpha<-120
    Scr=4;
elseif alpha>=-120&&alpha<-60
    Scr=5;
else
```

```
    Scr=6;
end
%Dwell time calculator=========================
function [ta,tb,t0]=T(Valpha,Vbeta,Scr)
X=sqrt(3)*Ts/Vdc*Vbeta;
Y=sqrt(3)*Ts/2/Vdc*(sqrt(3)*Valpha+Vbeta);
Z=sqrt(3)*Ts/2/Vdc*(-sqrt(3)*Valpha+Vbeta);

if Scr==1
    ta=-Z;tb=X;
elseif Scr==2
    ta=Z;tb=Y;
elseif Scr==3
    ta=X;tb=-Y;
elseif Scr==4
    ta=-X;tb=Z;
elseif Scr==5
    ta=-Y;tb=-Z;
else
    ta=Y;tb=-X;
end
%Duty cycle calculator=======================
function [Tda,Tdb,Tdc]=D(ta,tb,t0,Scr)
Taon=0.25*t0;
Tbon=Taon+ta/2;
Tcon=Tbon+tb/2;
if Scr==1
    Tda=Taon;Tdb=Tbon;Tdc=Tcon;
```

```
elseif Scr==2
    Tda=Tbon;Tdb=Taon;Tdc=Tcon;
elseif Scr==3
    Tda=Tcon;Tdb=Taon;Tdc=Tbon;
elseif Scr==4
    Tda=Tcon;Tdb=Tbon;Tdc=Taon;
elseif Scr==5
    Tda=Tbon;Tdb=Tcon;Tdc=Taon;
else
    Tda=Taon;Tdb=Tcon;Tdc=Tbon;
end
%=========================================
```